

Experimental and numerical analysis of stiffened curved plates as bottom flanges of steel bridges

Sara Piculin^a, Primož Može^a

^a Faculty of Civil and Geodetic Engineering, University of Ljubljana, Slovenia

Corresponding author:

Sara Piculin

Faculty of Civil and Geodetic Engineering, University of Ljubljana

Jamova 2

1000 Ljubljana, Slovenia

Tel: +386 1 4768 672

Email address: spiculin@fgg.uni-lj.si

ABSTRACT

This paper deals with the experimental and numerical evaluation of the buckling behaviour and ultimate resistance of stiffened transversally curved panels subjected to uniform axial compression. Furthermore, a verification procedure for curved stiffened panels is proposed that gives a good estimation of the maximum loads obtained from experimental and numerical tests. The procedure is in line with the design methodology of EN 1993-1-5, accounting also for panel curvature. Nine large-scale tests were performed on longitudinally and transversally stiffened plates made of high strength steel, namely S500 and S700. They were subjected to compressive stresses up to collapse. The nine specimens comprised of flat and curved plates that differed in material grade and geometric parameters, such as panel thickness, aspect ratio, size and shape of stiffeners. The effects of different parameters on the plate's resistance to pure compression are discussed. Moreover, a numerical model built in the general-purpose code ABAQUS is presented and verified against the test results regarding initial stiffness, ultimate resistance and failure mode. Numerical simulations (FEA), based on the test panel geometry, the measured initial geometric imperfections and elasto-plastic material characteristics from tensile tests, demonstrate very good agreement with experimental results.

Keywords: stiffened curved plates; experimental investigation; FEM; initial imperfections; steel bridges; uniform compression.

1 Introduction

New aesthetic forms of modern steel and steel-concrete composite bridges increased the interest in the research of cylindrically curved plates. Furthermore, curved plates as structural elements are widely used in many other applications, such as marine, offshore and fibre composite fuselage structures. In practical bridge design, curved plates usually represent the lower flange and are longitudinally welded to vertical or inclined web plates in order to form a closed box-section. In contrast to the classic approach, where the box girder is composed of stiffened flat plate elements and designed according to EN 1993-1-5 [1], the design of curved plates is not covered by the Structural Eurocodes. A recent survey by Biscaya da Graça *et al.* [2] identified almost 20 roadway, railway and pedestrian bridges, where curved shapes of bottom flange plates were adopted. In most of the aforementioned cases, the curvature of the identified bridges falls out of the scope of the design code EN 1993-1-5 that is limited to flat plates. Plate elements may be considered as flat, if the radius of curvature R satisfies a given limit R_{lim} depending on panel width b and plate thickness t :

$$R_{lim} \geq b^2 / t \quad (1)$$

The cable-stayed Escaleritas Viaduct [3] and the case study by Reis *et al.* [4] on a continuous girder bridge (see Fig. 1) represent typical applications of a transversally curved plate in a bridge box cross-section. In both cases, the geometry exceeds considerably the limit from Eq. (1). In addition, it has been proven by several authors that curved panels have different characteristics compared to the flat ones [5,6]. In fact, in most cases, the increased cross-sectional moment of inertia leads to a higher resistance compared to flat plates [7]. Therefore, a sophisticated FEM analysis is necessary in order to properly calculate the ultimate resistance of curved plates as individual members of box cross-sections.

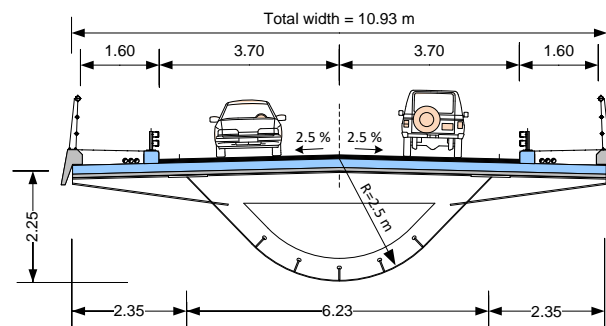


Fig. 1. Cross-section with transversally curved bottom flange [4].

In general, plate elements as parts of box girders are predominantly subjected to in-plane loading. A uniform compressive stress distribution arising from longitudinal bending is a typical loading situation for bottom plates of box girders near internal supports. Furthermore, plate-like and shell-like structures are usually designed as slender (cross-section class 4 acc. to EN 1993-1-1 and design acc. To EN1993-

1-5 and EN1993-1-6, respectively) and are therefore prone to stability phenomenon, in this case specifically to buckling due to direct compressive stresses. Although some interaction between shear and compressive stresses may be expected due to the curved shape of the lower flange, this study focuses on plates subjected to uniform axial compression. The “effective width method” approach from EN 1993-1-5, where direct and shear stresses are checked separately, is followed. For ultimate shear resistance of curved steel panels, reference is given to Ljubinković *et al.* [8].

The design of plated structures should meet several requirements, such as weight minimization and maximization of the buckling resistance. As shown by Oliveira Pedro *et al.* [9], in the design of highway bridges steel weight can be reduced up to 25 % by using high strength steel (HSS) instead of mild strength steel, although the plate thickness reduction leads to decks more susceptible to local buckling. In order to increase the buckling resistance by a small addition of weight, curved plates are usually stiffened with evenly spaced longitudinal stiffeners. When the stiffeners possess sufficient flexural stiffness, only local buckling of subpanels between stiffeners develops. Otherwise, for weaker stiffeners, the panel fails predominantly in a global buckling form, where the longitudinal stiffeners are involved in the overall buckling of the panel between transverse stiffeners. For a stiffener with medium stiffness, a combination of local and global buckling occurs. Note that transverse stiffeners have to be rigid enough to give support to the longitudinal stiffeners [10]. For flat plates, EN 1993-1-5 defines global buckling as a combination of plate-like and column-like buckling of the stiffened plate. Depending on the interaction between the two behaviours, a reductions factor is defined that reduces the cross-section area of the stiffened panel together with the reduction factor related to local buckling of subpanels. The background information is given in [11].

The lack of practical design rules for stiffened and unstiffened curved plates under in-plane stresses drove several authors to study their behaviour with a scope of proposing methods for the calculation of elastic buckling stress and ultimate resistance. A detailed review of these studies and the proposed methods for curved plates under generalized in-plane stresses is given by Martins *et al.* [12]. Herein, a few more recent ones are exposed. Seo *et al.* [13] derived closed-form expressions to predict the ultimate compressive strength of curved stiffened plates for marine and offshore applications. Similarly to other studies in this field, authors in [14] performed a parametric study on a so-called double span/double bay model with one stiffener that does not account for the effects of global buckling. In bridge engineering applications, Martins *et al.* [15,16] studied unstiffened cylindrically curved panels under compressive stresses and proposed design approaches in accordance with the current rules from EN 1993-1-5. Tran *et al.* [7,17] proposed two methods to compute the ultimate strength of stiffened curved panels under uniform compression and concluded that curvature increases the second moment of inertia, which leads to higher elastic buckling stress and higher ultimate resistance. They proposed a simple and rather conservative methodology for the estimation of the ultimate strength [7] that relies on a column-like approach derived from the model of resistance of stiffened flat plates. The second method [17] follows

a statistical approach based on a design of experiment method. The proposed formula for computing the ultimate load factor is limited to open section stiffeners. Later in this paper, the methods from Martins *et al.* [15,16] and Tran *et al.* [7] are explained in detail and compared to maximum loads obtained from experimental tests.

However, none of the above mentioned studies and proposed methods has any experimental background. Unlike slender flat plates with stiffeners, where quite some experimental work has been done recently, e.g. [16–19], experimental tests on curved plates are not so numerous. Cho *et al.* [22] performed axial compression test on six curved stiffened plates representing the bilge strikes of container ships and found positive effects of curvature on the ultimate strength. Nevertheless, due to the specific geometry and material of the specimens that were based on a ship survey, the results of the study are not directly applicable to bridge design. To the author's knowledge, the recent experimental investigations by Ljubinkovic *et al.* [23,24] are the only dealing with curved plates for bridge application. They performed compression test on cylindrically curved panels and bending tests on two bridge segments with transversally curved bottom flanges. It is important to point out that in bridge segments, failure was concentrated in the curved bottom flange close to the mid-support where the highest compressive stresses develop. All the aforementioned statements underline the need for an experimental evaluation of axially loaded stiffened curved plates as parts of bridge deck cross-sections.

Hence, this paper presents experimental tests on nine large size stiffened curved plates subjected to uniform compressive stresses together with numerical simulations. Based on of two methodologies recently published by Martins *et al.* [15,16] and Tran *et al.* [7], a verification procedure for curved stiffened panels is proposed that is in line with the design methodology of EN 1993-1-5, accounting also for the positive effects of panel curvature. The tests are part of an extensive research project aiming to verify the proposed design methodology through a comprehensive parametric study performed on the numerical model calibrated on test results.

The article is organised as follows. In Section 2, the specimen geometry, experimental test setup and measuring techniques are described together with the main test results. Subsequently, in Section 3, the numerical simulations of experimental tests are presented with emphasis placed on modelling the initial geometric imperfections and residual stresses. Finally, Section 4 presents two methodologies for the calculation of the ultimate resistance for flat plates from EN1993-1-5 and for curved plates from literature. Comparison between verification procedures, numerical and experimental results is made.

2 Experimental tests

Experimental tests on large-scale specimens are aimed at examining the ultimate resistance and structural behaviour of longitudinally stiffened curved panels in compression. Within the experimental investigation, nine isolated stiffened steel plates made of high strength steel, namely S500 and S700, were tested, two of them were flat and the other seven were curved. They were loaded in uniaxial compression in the vertical direction. Specimens with different parameters were included in the investigations in order to examine their effects on the ultimate resistance. Finally, the experimental results were the basis for the validation of the numerical model.

2.1 Geometry and material properties

The basis for the test specimen geometry definition was a bridge case study performed by Reis *et al.* [4], where a box girder was adopted, formed from a curved bottom flange with a radius of 2.5 m and longitudinally stiffened with flat stiffeners. The dimensions of the bridge were chosen within the rules of common engineering practice for bridge design. The tested specimens represent a part of the lower flange and are scaled down approximately five times with respect to the case study, due to the limited piston capacity and laboratory height limitations. The scaling factor was defined based on preliminary numerical calculations considering increased yield strength of material and did not affect the plate slenderness.

For practical reason, to avoid changing the test setup, the overall test specimen geometry was the same for all tests. The general specimen geometry is presented in Fig. 2 together with the relevant parameters required for the definition of the stiffened plate, both flat and curved. Additionally, the curvature of a cylindrically curved panel is denoted with global curvature parameter Z that was first proposed by Batdorf [25] and later adopted by several authors [7,15], by removing the Poisson's coefficient:

$$Z = \frac{b^2}{Rt} \quad (2)$$

In case of stiffened plates, the local curvature parameter for unstiffened subpanels is defined by the following expression:

$$Z_{loc} = \frac{b_{loc}^2}{Rt} \quad (3)$$

Some of the parameters were kept constant for all specimens, namely, panel width $b = 612$ mm, panel height $L = 1764$ mm and the transverse stiffeners height and thickness, $h_{st} / t_{st} = 90$ mm / 4 mm. Seven curved and two flat panels were tested, all stiffened with two longitudinal and one or three transverse stiffeners, resulting in two different aspect ratios of longitudinally stiffened panels between transverse stiffeners $\alpha = a / b$. Cut-outs were made in the transverse stiffeners to allow for the continuity of the

longitudinal stiffeners. The varying parameters are listed in Table 1, where specimens are denoted with C for curved panels and F for flat panels. Specimen 6C is stiffened with T-shaped longitudinal stiffeners (Fig. 3), all other specimens have flat stiffeners. Longitudinal stiffeners are continuous as they pass through the openings in transverse stiffeners. For all specimens, subpanels between stiffeners are classified as slender class 4 cross-sections with relative slenderness $\overline{\lambda}_p$ ranging between 0.8 and 1.4.

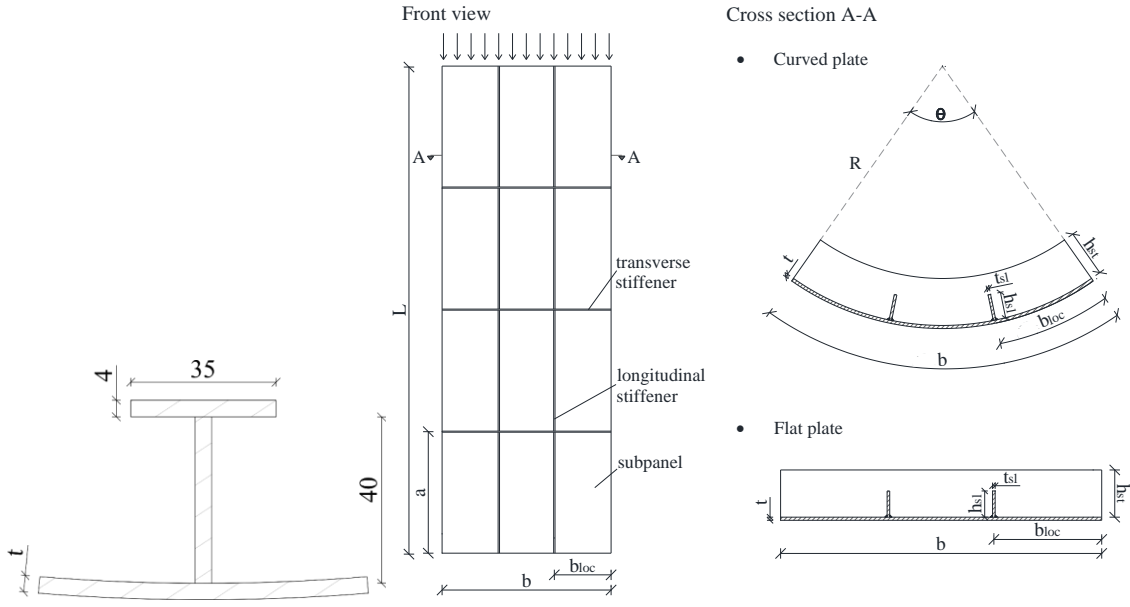


Fig. 2. Test specimen geometry.

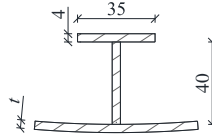


Fig. 3. Dimensions of T stiffener in [mm].

Table 1. Nominal values of geometric and material properties of test specimens.

Specimen	Plate						Subpanel		Longitudinal stiff.	
	Material	R [mm]	t [mm]	a [mm]	α	λ_p	Z_{loc}	h_{sl}/t_{sl} [mm]	Material	
curved	1C-1	S-1	500	6	432	0.71	0.81	12	50/5	S-3
	1C-2	S-1	500	6	432	0.71	0.81	12	50/5	S-3
	2C*	S-4	500	6	432	0.71	0.81	12	50/4	S-5
	3C	S-2	500	4	432	0.71	1.22	18	50/5	S-3
	4C	S-5	500	4	432	0.71	1.44	18	50/4	S-5
	5C	S-2	500	4	876	1.43	1.22	18	50/6	S-1
	6C	S-2	500	4	876	1.43	1.22	18	T	S-2
flat	1F-1	S-1		6	432	0.71	0.81		50/5	S-3
	1F-2	S-1		6	432	0.71	0.81		50/5	S-3

* Specimen 2C was designed as S700. After the fabrication, material tests were performed, and the plate turned out to be S500. Hence, the stiffeners are S700 and the plate is S500.

The test specimens were fabricated from five different steel plates. The standard tensile tests according to [26] were carried out to determine the elastic-plastic stress-strain relation for each plate in order to obtain more accurate material characteristics for the successive numerical simulations. Two tensile coupons were extracted from each plate according to [26]. The results of tension tests are summarized in Table 2, where t_m denotes the actual measured thickness of the plate, $R_{p0.2}$ denotes the characteristic plastic strength at the strain of 0.02%, R_{eH} the high static value of the yielding strength, R_m the ultimate tensile strength, ε_u the uniform strain and ε_f the fracture strain.

Table 2. Measured material properties for all five steel plates.

	Material		t_m [mm]	$R_{p0.2}$ [N/mm ²]	R_{eH} [N/mm ²]	R_m [N/mm ²]	ε_u [%]	ε_f [%]
S-1	S500MC	1	5.84	542	-	653	10.06	21.48
		2	5.84	539	-	653	10.02	21.18
S-2	S500MC	1	3.87	-	576	642	12.00	23.76
		2	3.87	-	581	647	13.15	24.66
S-3	S500MC	1	4.84	-	553	642	11.73	23.01
		2	4.84	-	554	647	11.56	23.16
S-4	S500MC	1	5.85	542	-	659	11.78	22.03
		2	5.84	541	-	658	10.30	22.18
S-5	S700MC	1	4.05	-	768	828	11.27	21.93
		2	4.06	-	767	827	11.48	22.23

2.2 Test setup and procedure

The test setup indicated in Figs. 4 and 5 was carefully designed to achieve uniform compression in the panel and to avoid any eccentricity during load application that would result in an additional edge bending moment. The hydraulic piston was installed on the main testing frame together with the vertically positioned test specimen. The curved edges of the specimen were fixed; longitudinal edges were simply supported. For this purpose, the curved edges of the specimens were welded to stiff, 30 mm thick end plates (Fig. 6) and bolted to stiff HEM300 girders that served for uniform load and reaction distribution. The girders were supported out-of-plane to the reaction wall with support arms. A cast nylon (PA6G) low friction plate was used on the upper girder to enable the free vertical movement of the specimen. The bottom girder distributed the reaction forces to the floor through a concrete block. The specimen's vertical edges with a width of 1 mm were positioned into linear rotational supports that were designed in order to restrain only the out-of-plane displacement and to allow the vertical and the lateral displacement together with the rotation around the vertical axis. The linear supports were similar to those used by Zizza [27] and Pourostad *et al.* [28]. They were connected to vertical columns that were adequately supported in the lateral and out-of-plane direction.

The axial compression load was applied directly on the geometric centre of the specimen's cross-section area using a hydraulic piston with maximum capacity of 3000 kN. The load was uniformly distributed

to both the panel and the longitudinal stiffeners. The tests were displacement controlled, with monotonously increased displacement up to collapse. After the elastic preloading phase, where the specimen was loaded in elastic range up to approximately 10% of the anticipated maximum load and then unloaded, the rate of displacement was 0.01 mm/s. During stops, photos were taken for the photogrammetric measurements.

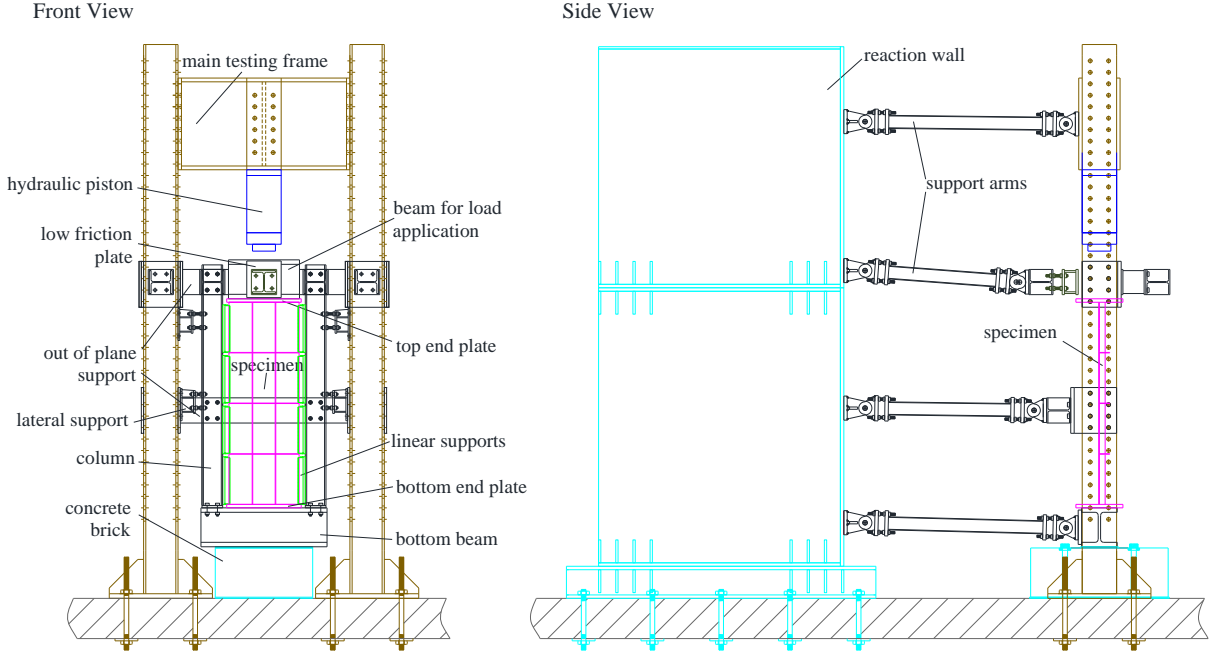


Fig. 4. Schematic representation of the test layout.

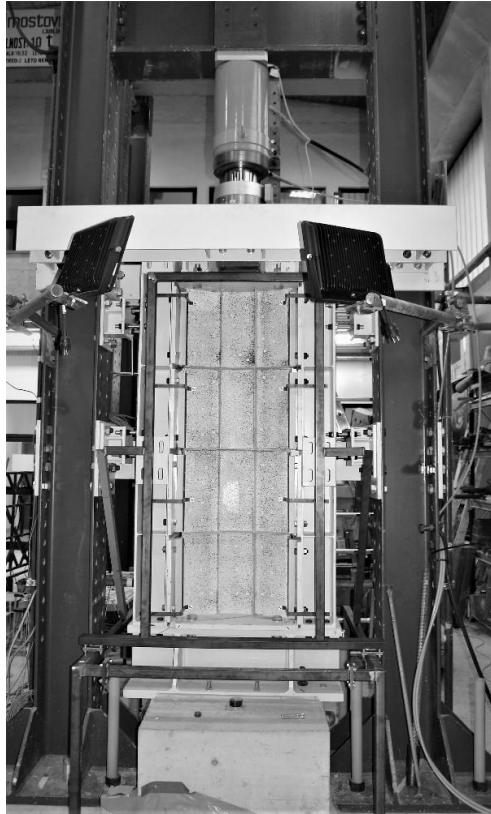


Fig. 5. Laboratory test setup with specimen 1C-1 in position.



Fig. 6. Specimen 1C-1 with end plates welded to curved edges.

2.3 Measurements

For the purpose of numerical simulations, the initial geometry of the specimens was measured by a structured light portable 3D scanner, namely ATOS Compact Scan 5M by GOM. The measured out-of-plane imperfections for specimens 1C-1 and 1C-2 at two different heights are plotted in Fig. 7. The measurements were further used for the interpolation of initial geometric imperfections in the finite element model.

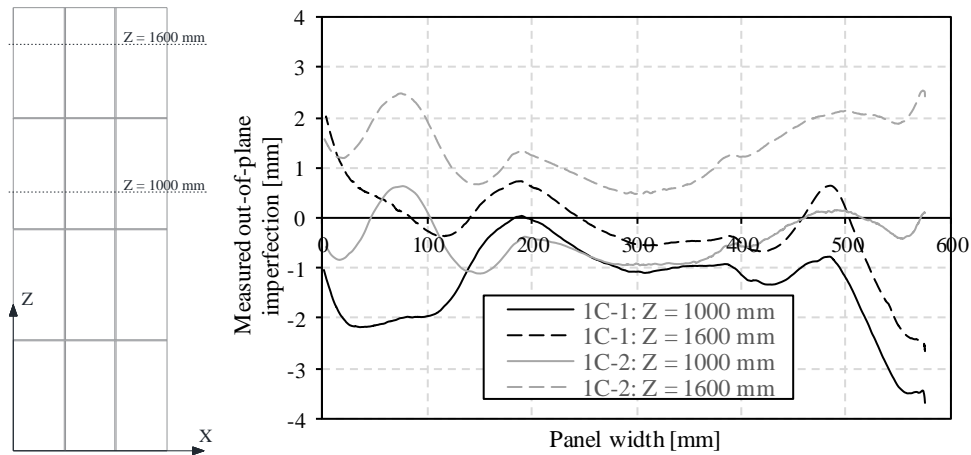


Fig. 7. Measurements of initial imperfections of specimens 1C-1 and 1C-2 at two heights.

During the tests, the following quantities were measured:

- applied load F measured by a load cell (Fig. 8),
- one-dimensional strains of 18 characteristic points of the panel and the stiffeners (for the positions, see Fig. 9),
- lateral and out-of-plane displacements of the supporting structure measured continuously with linear transducers (LVDTs) in 8 discrete points,
- vertical displacement v and out-of-plane displacement w of the panel measured continuously with LVDTs in 2 discrete points (Fig. 8),
- displacement field of the panel in the out-of-plane direction calculated from the photogrammetric measurements.

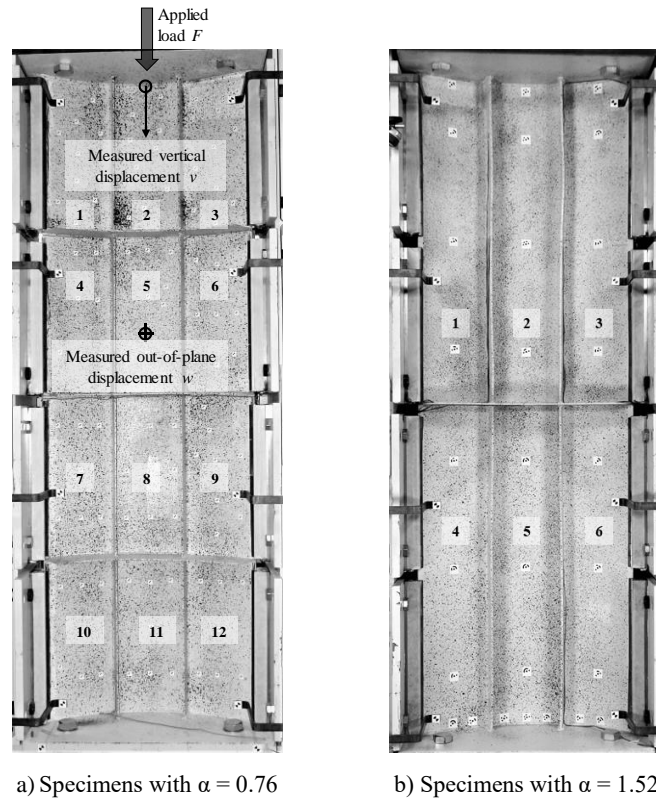


Fig. 8. Position of applied force F and measured displacements v and w ; notations of subpanels.

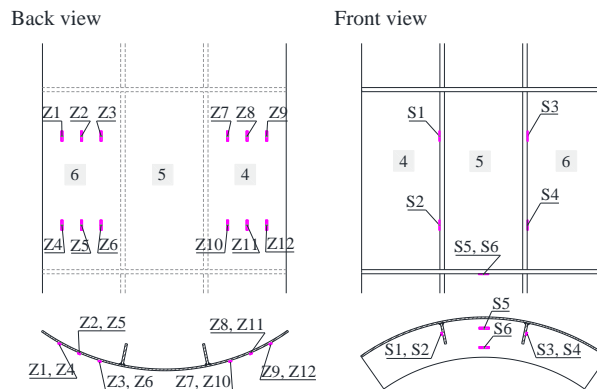


Fig. 9. Position of strain gauges on the back and front sides of the specimen with $\alpha = 0.76$.

For the photogrammetric measurements, an artificial texture was applied by paint to the stiffened face of each specimen to produce a dense point cloud. In addition, 40 coded targets were attached to the panel. The load application was paused according to a predefined protocol. During each pause, a block of 4×3 images of the specimen was taken using Nikon D610 DSLR camera. From each image block, the coordinates of the coded targets were calculated. This enabled tracking of the displacements in discrete points at each loading step. From the calculated point cloud, the out-of-plane displacements of the specimen at different loading steps were calculated. The procedure is described in more detail in Grigillo *et al.* [29]. Due to the coded targets and painted point cloud, the position of strain gauges was limited to the back side of the panel.

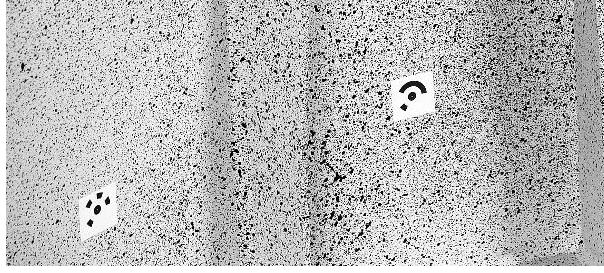


Fig. 10. Specimen painted in random speckle pattern and coded targets.

2.4 Test results

Some of the main test results are presented in the following sections. The applied load F and measured vertical displacement v plotted in the graphs of the following sections are displayed in Fig. 8. For a clearer description of the failure modes, subpanels of the specimens are numbered.

2.4.1 Load-shortening curves and ultimate resistance

The response curves for all nine tests are presented in Fig. 11, where the ultimate resistance of each specimen is determined as the maximum of the load-shortening curve. The specimens with a panel thickness of 6 mm are presented on the left and the specimens with a panel thickness of 4 mm are presented on the right figure. Vertical displacement v at the load application point is plotted on the abscissa and the applied load F on the ordinate axis. Due to the load application stops, the curves are not completely smooth.

The initial inclination of the curves for specimens with plate thickness $t = 6$ mm, i.e. the initial stiffness of the panels, is comparable. Slightly lower stiffness is observed for specimen 2C. The difference may be attributed to a thinner longitudinal stiffener. All specimens showed a linear elastic response up to a high load level. The stiffness gradually decreased as the plates passed over to the plastic range. The highest capacity was attained for specimen 1C-2, followed by 1C-1 with a 4.6 % lower capacity. The two specimens had the exact same nominal geometry and material, so the difference in the ultimate resistance may be attributed to different geometric imperfections (Fig. 7) and to the inevitable minor variation in the position of the applied force. The two flat panels, namely 1F-1 and 1F-2, had the same nominal geometry and material as 1C-1 and 1C-2, and consequently the same cross-section area, the only difference was the curvature. The ultimate force obtained by the flat panels was 13 % to 19 % lower compared to the curved panels. This confirms the observations made by previous authors [7,16] that curvature increases the ultimate strength of panels.

The initial stiffnesses of slender panels, e.g. specimens with plate thickness $t = 4$ mm, slightly differ, since all four specimens have some differences in the nominal geometry and material. In all cases, an almost instantaneous drop of resistance is observed, due to local instability of subpanels. The first drop is followed by an increased resistance and finally, the ultimate resistance is reached due to local buckling

of several subpanels and longitudinal stiffeners. The highest capacity was reached by specimen 4C due to the highest steel grade, followed by the other three specimens that had similar capacity. Both cases with larger aspect ratios, namely 5C and 6C, yielded a similar resistance compared to specimen 3C, regardless of the doubled value of aspect ratio. This is in line with the conclusions made by the authors in the previous numerical study [6], where it was shown that by increasing the aspect ratio above $\alpha = 1$, the ultimate resistance remains nearly constant or slightly decreases.

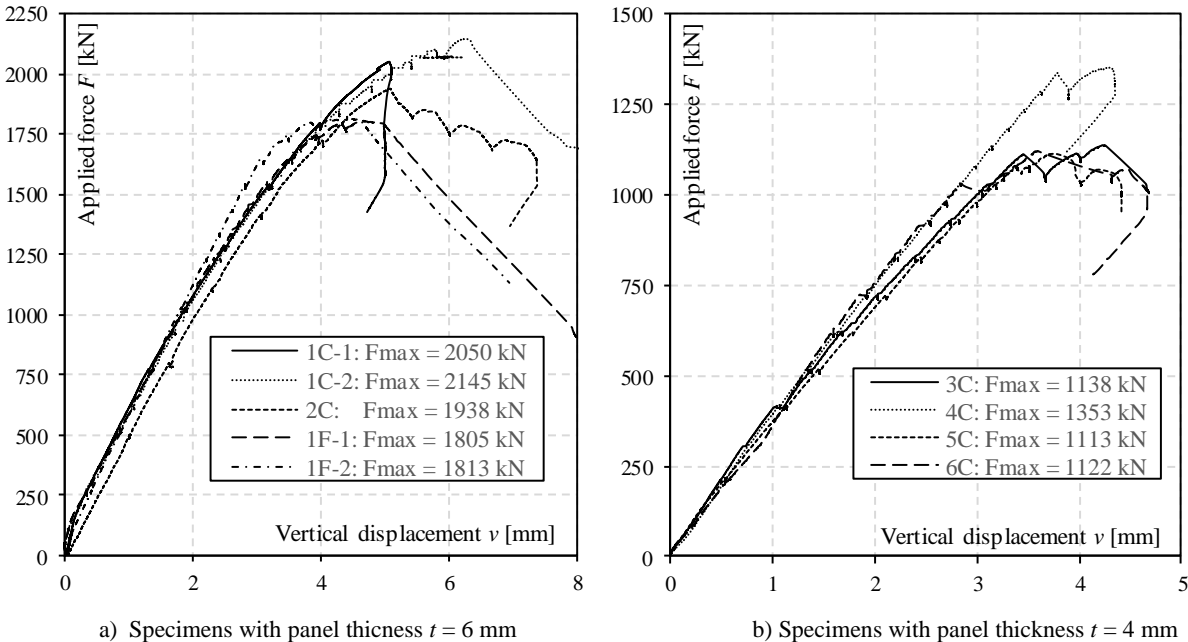


Fig. 11. Experimental load-shortening curves for all nine specimens

2.4.2 Out-of-plane deflections and collapse mechanisms

Fig. 12 shows the evolution of the out-of-plane displacements in contour plots for specimen 2C. The loading steps are marked on the load-shortening curve. In Fig. 13, the out-of-plane deformation lines at the cross-section with the largest displacements are plotted. The results were obtained by photogrammetric method and do not contain the initial imperfections. After a small global deformation of the panel, the specimen resistance is exhausted due to local buckling of subpanels 10, 11 and 12 (see Fig. 8). In addition, torsional buckling of longitudinal stiffeners may also be observed in Fig. 14, showing failed specimen 2C after unloading.

Out-of-plane displacements of specimen 3C are presented in Figs. 15, 16. The results indicate that the local type of buckling shape prevails. In addition to the local buckles in nearly all the subpanels, there is a certain degree of stiffener deflection. The first drop in the load-shortening curve happened after the first half-wave due to the buckling of subpanel 4. After the drop, the resistance of the specimen increased again. The failure occurred after the buckling of the adjacent subpanels.

According to [12], similarly to flat plates, stiffened cylindrically curved plates may exhibit four different buckling modes, namely global buckling of the curved panel, beam-column-type buckling of the panel-stiffener system, local buckling of the unstiffened subpanel between stiffeners and local buckling of stiffeners. The experimental results for curved specimens indicate that a local collapse mechanism prevailed in all cases, in combination with torsional buckling of longitudinal stiffeners. The stiffeners possessed sufficient bending stiffness to induce local buckling of subpanels for all specimens. Before the failure, a small global deflection of the stiffened plate was observed for specimens with higher panel thickness, e.g. 1C-1, 1C-2 and 2C (Fig. 13), but the amplitude was approximately 5 times smaller compared to local buckling deflections after failure. The local failure mechanism is in all cases very similar to the so-called “Roof-shape mechanism”, typically encountered in flat plates subjected to in-plane compressive stresses [30,31], see Fig. 17.

Figs. 18 and 19 show the evolution of the out-of-plane displacements for the flat specimen 1F-1. Buckling patterns were starting to form from the 9th loading step up to the maximum resistance that was met short after the 11th loading step. After that, the buckling patterns induced a shift of the centroid of the deformed shape of cross-section relative to the centre of gravity of the undeformed cross-section. With the increasing deformations, shift e_N increased, resulting in an additional bending moment $\Delta M = e_N F$, finally leading to bending deformation. After the specimen failure, the bending moment induced relatively large lateral reaction forces that led to the rotation of linear supports, allowing a global failure of the vertically unsupported specimen 1F-1. The bending failure mechanism may be observed in Fig. 20 together with the torsional buckling of the longitudinal and the transverse stiffeners. Very similar behaviour was observed for specimen 1F-2.

Bending failure was observed only for flat specimens, while for curved specimens, the additional bending moment due to load eccentricity ΔM did not have any significant effect on the cross-sectional resistance. In point of fact, due to its curved geometry, section modulus W_y of a curved cross-section is considerably higher compared to a flat one, resulting in a higher bending resistance. Comparing 1C-1 to 1F-1, it is approximately five times higher.

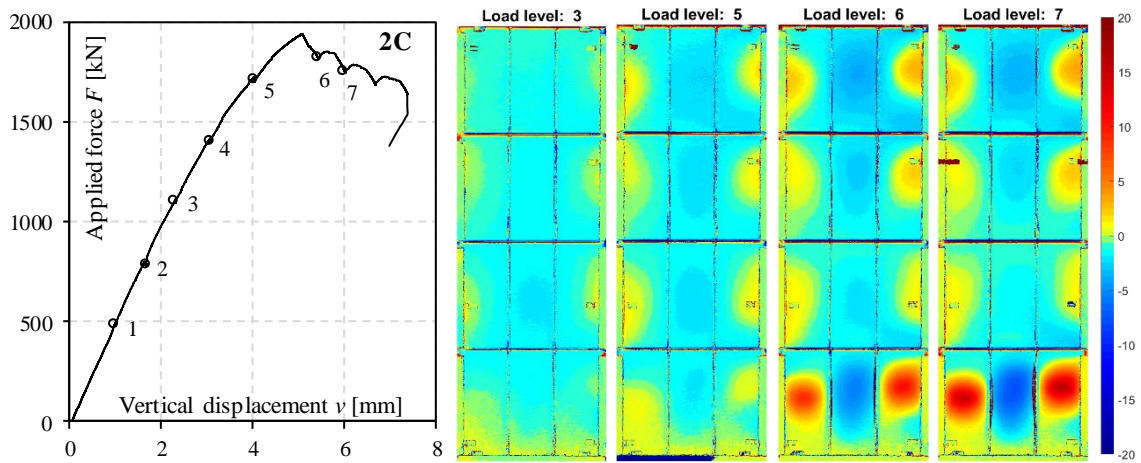


Fig. 12. Evolution of out-of-plane displacements [mm], specimen 2C.

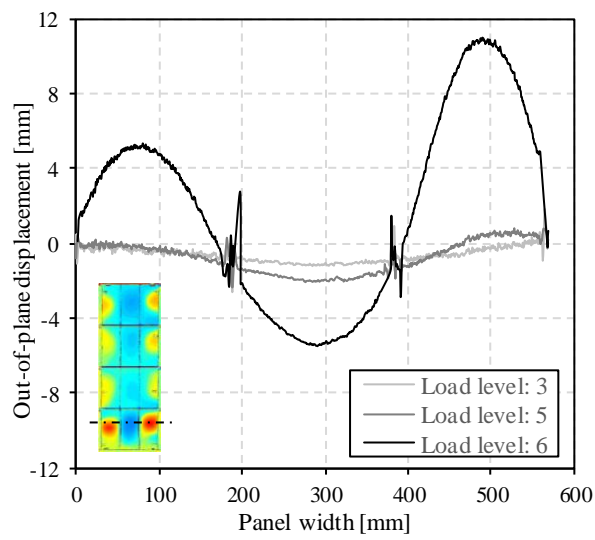


Fig. 13. Out-of-plane deformation lines at different load levels, specimen 2C.

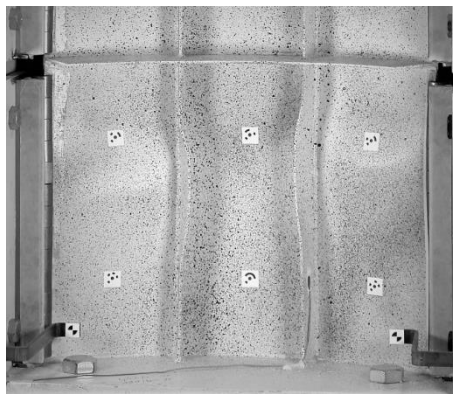


Fig. 14. Specimen 2C after unloading.

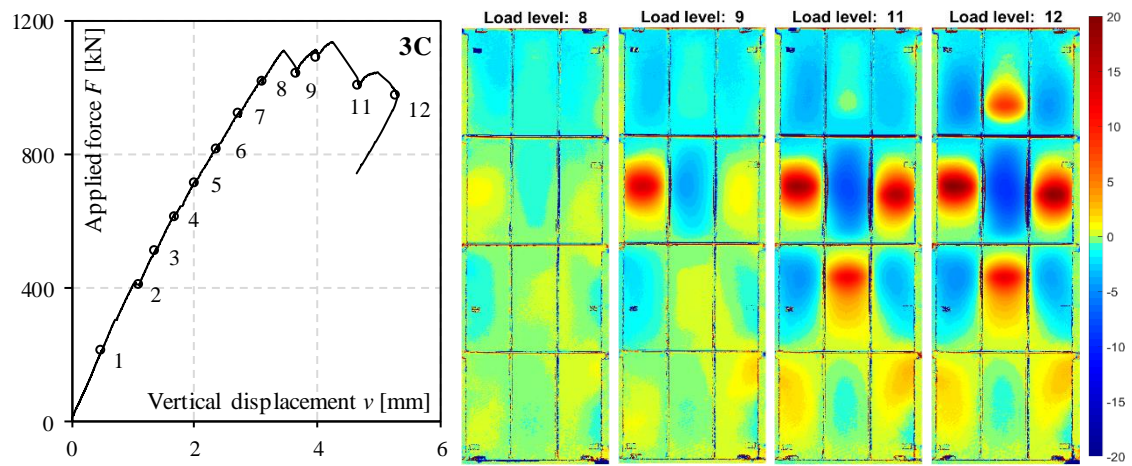


Fig. 15. Evolution of out-of-plane displacements [mm], specimen 3C.

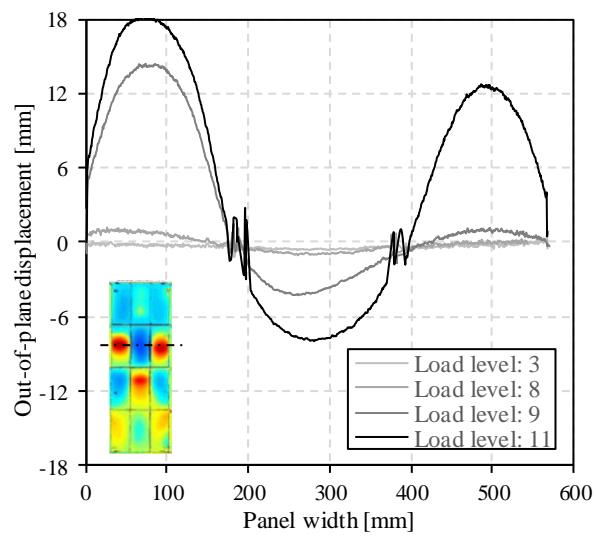


Fig. 16. Out-of-plane deformation lines at different load levels, specimen 3C.

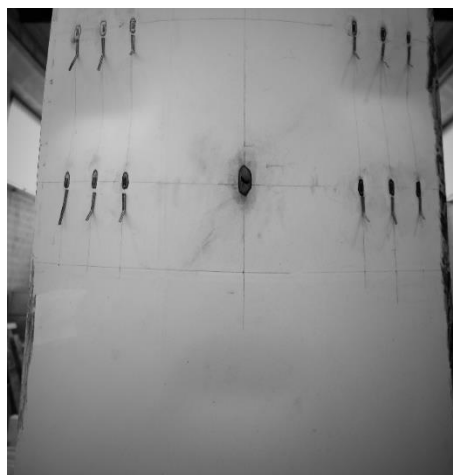


Fig. 17. Specimen 3C after unloading.

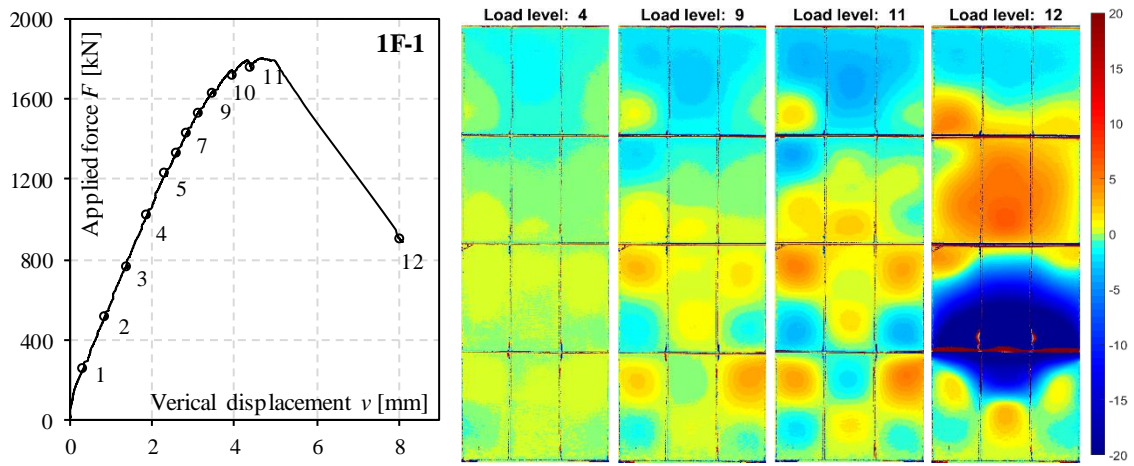


Fig. 18. Evolution of out-of-plane displacements during loading [mm], specimen 1F-1.

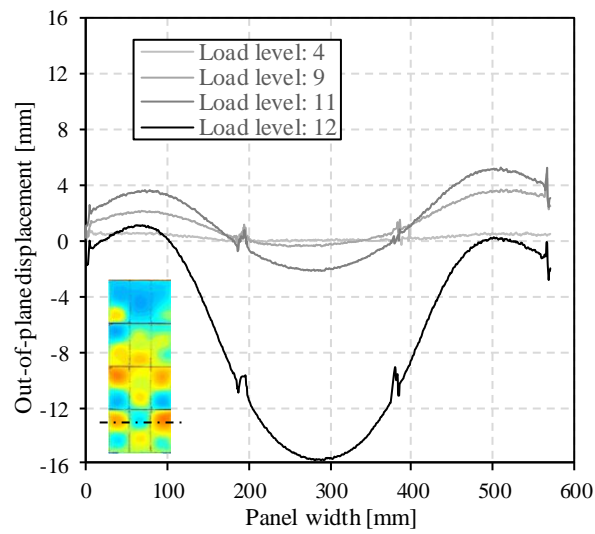


Fig. 19. Out-of-plane deformation lines at different load levels, specimen 1F-1.



Fig. 20. Specimen 1F-1 after unloading.

2.4.3 Strains

Strain development was measured with one-dimensional strain gauges (SGs) in 18 characteristic points (Fig. 9) of stiffeners and subpanels 4 and 6 (Fig. 8). In most cases, the location of SGs did not coincide with the subpanels where failure had occurred. Fig. 21 presents the strains and the position of SGs in specimen 1C-1. The failure was concentrated in subpanel 1. In the first phase, the measured compression strains are elastic and almost constant along the panel cross-section. At the ultimate force, the strain in DZ8 and DZ9 is around 5.5 ‰, which is rather above the yield strain of 2.6 ‰. In the longitudinal stiffeners, the upper two SGs, namely DS1 and DS3, show the highest strains that also exceed the yield strain. Similar results were observed for all specimens with panel thickness 6 mm, namely 1C-2, 2C, 1F-1 and 1F-2. At ultimate force, in some parts of the plate the strains exceeded the yield strain. In these cases, global failure can be associated with the combination of local buckling and yield of material.

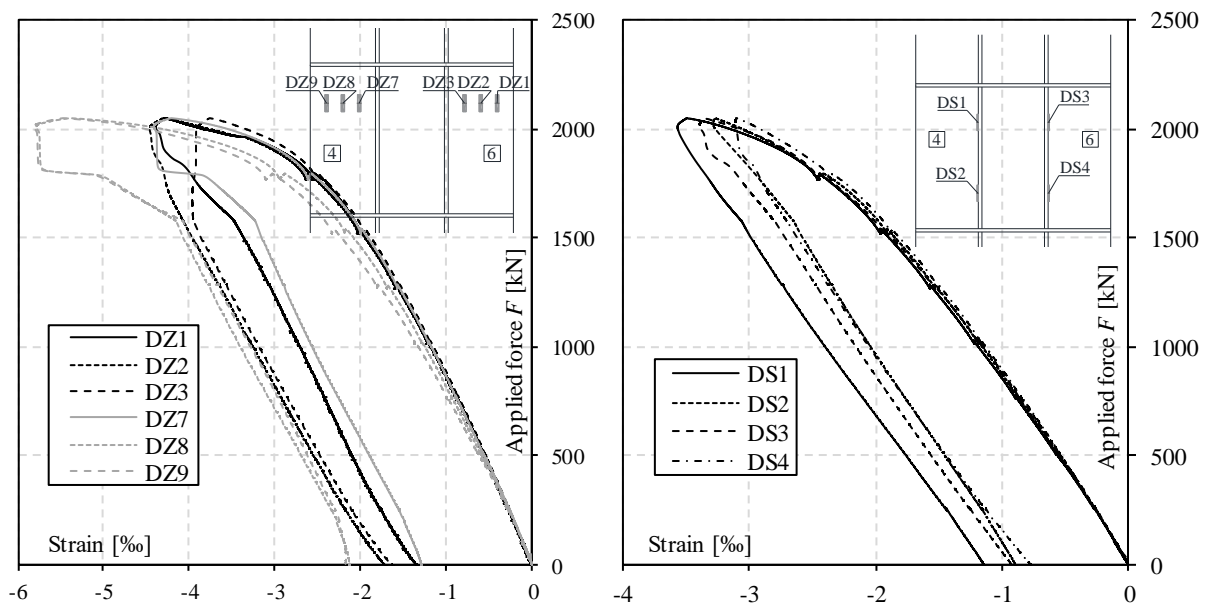


Fig. 21. Strain measurement, specimen 1C-1.

Vice-versa, for specimens with higher panel slenderness, namely 3C, 4C, 5C and 6C, the majority of the measured strains did not exceed the yield strain. In Fig. 22 the strains vs. vertical displacement for specimen 3C are plotted. In this case, buckling happened exactly in the panel where strains were measured. In the first phase, the compression strains are again elastic and almost constant through the whole cross-section, increasing gradually with the increased vertical displacement. The first half-wave due to buckling occurred in subpanel 4 affecting strains DZ8-DZ10 that instantaneously changed from compressive to tensile. After the ultimate force had been reached, the same occurred in subpanel 6, where the second half-wave appeared. The highest strain was reached in DZ8, where the yield strain of 2.8 ‰ was exceeded only after the global failure of the specimen. The majority of the measured strains showed that also in the post-buckling phase, the panel was in the elastic region. Consequently, for

specimens with thinner panels, failure may be associated mostly to local buckling of subpanels in combination with torsional buckling of longitudinal stiffeners.

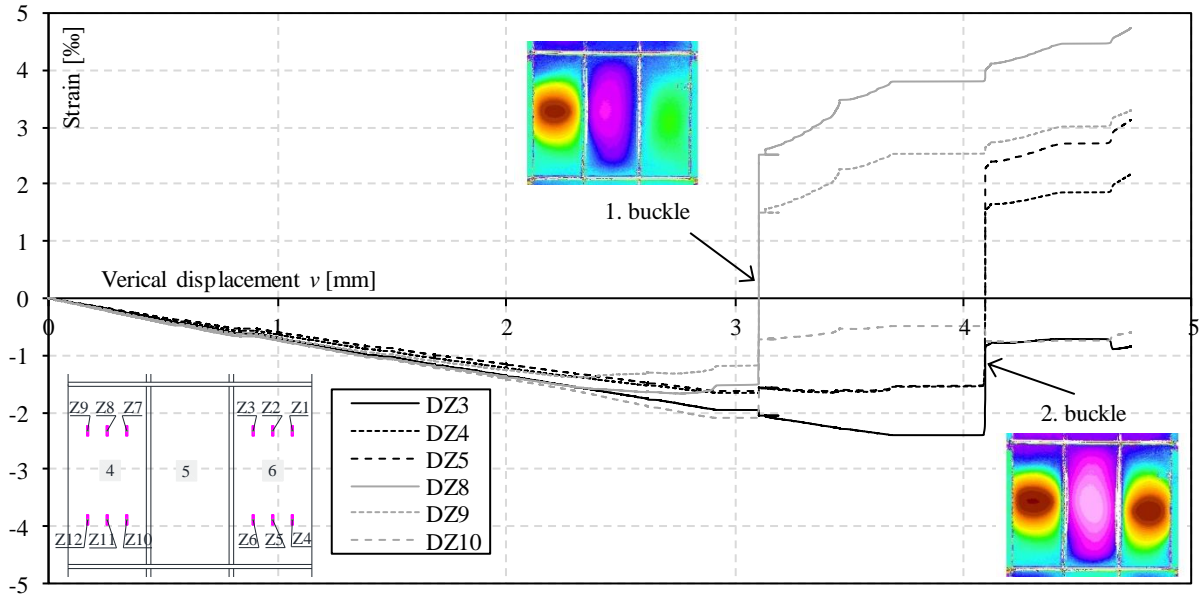


Fig. 22. Strain measurement, specimen 3C.

3 Numerical simulations

3.1 Numerical model

The numerical model for the experimental test simulation was built in the finite element software ABAQUS [32], where a fully nonlinear analysis with initial imperfections (GMNIA) and realistic boundary conditions was performed. Both buckling and collapse behaviour are involved in the specimen response; therefore, static equilibrium in the analysis was found by using arc length method. The test specimens were discretized using four node shell elements with reduced integration (S4R). The size of the finite elements was defined based on a preliminary convergence study and set up to approximately 12 mm. The FE model mid-plane geometry followed the nominal specimen dimensions presented in Section 2.1, except for the thicknesses, which were taken as measured, see Table 2. The numerical model simulated realistic boundary conditions from experiments. The curved edges of the panel were fixed, except the free vertical displacement of the top edge in the direction of the load application. Longitudinal edges were simply supported with the non-restrained circumferential and vertical displacement. The loading was controlled by a vertical displacement of the cross-section's centre of gravity, which was coupled to the nodes from the top edge, including both the plate and the longitudinal stiffeners.

The structural steel was modelled with an elasto-plastic material model defined according to static values of tension tests (Table 2). For the application in the FE model, the stress-strain diagrams of the five different materials were transformed in the form of Cauchy stress and logarithmic strain, see Fig. 23.

The elastic modulus was set to $E = 210 \text{ GPa}$ and Poisson's ratio to $\nu = 0.3$. The material model was verified with an FE simulation of the standard tension test and very good correlation between numerical and experimental results was achieved, except for the deviation in the rounded part of the curve that is presented on the enlarged diagram in Fig. 24. To account for a rounded stress-strain curve, which is typical for HSS and stainless steels, the two-stage Ramberg-Osgood model might be used, as in [33], but Abaqus includes only a one-stage model that is not properly accounting for the HSS strain hardening.

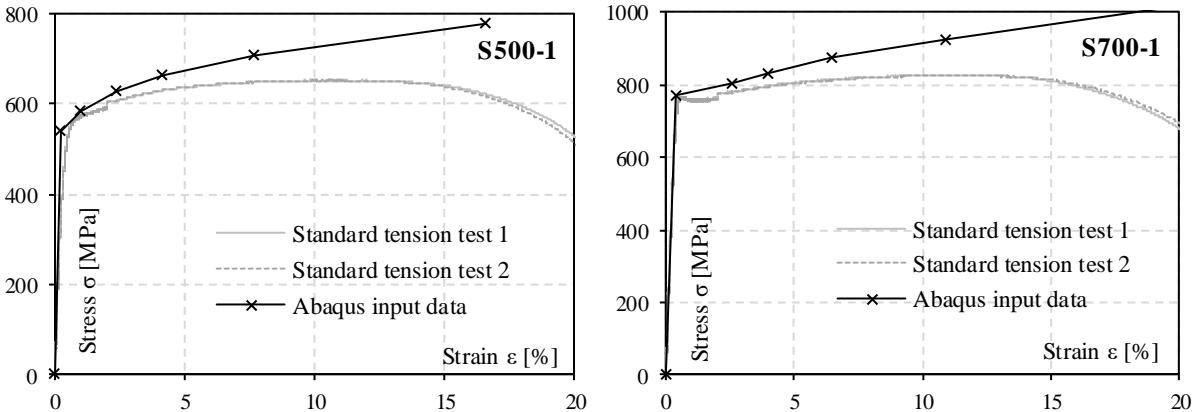


Fig. 23. Stress-strain curves for two of the five materials.

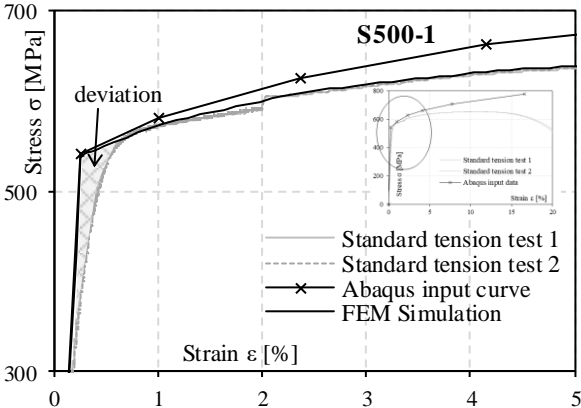


Fig. 24. Enlarged diagram of the rounded stress-strain curve for S500-1.

3.2 Initial imperfections

Initial imperfections come from two different origins, namely geometric imperfections and residual stresses. The effects of the two types of imperfections are in many cases quite different; therefore, to achieve higher accuracy of the simulations, in this study, they are considered separately. On the other hand, general guidelines for modelling initial imperfections given in EN 1993-1-5 [1] allow the combination of both effects by applying the equivalent geometric imperfections method. Hence, to compare their effects, these two approaches were used for modelling initial imperfections. In Model 1, the residual stresses and measured geometric imperfections were modelled separately. In Model 2,

equivalent geometric imperfections were applied according to the recommendations from Annex C in EN 1993-1-5.

The initial geometry of the tested panels was measured using a 3D scanner. The result of the scanning was a matrix of approximately 2×10^6 points that represent the difference between the nominal and the realistic geometry of the specimens. Geometrical imperfections were introduced in the shell finite element model by means of appropriate modifications of node coordinates. As the experimental grid used for the initial geometry measurement was very dense and did not coincide with the adopted finite element mesh, an interpolation procedure was performed to determine the nodal values. For this purpose, the kriging method that can handle unevenly distributed spaced data was performed for all nine specimens. An in-depth description of the method is given in [34,35]. The geometry of the stiffeners was considered as perfect. Two examples of the amplified estimates on the finite element mesh are presented in Fig. 25.

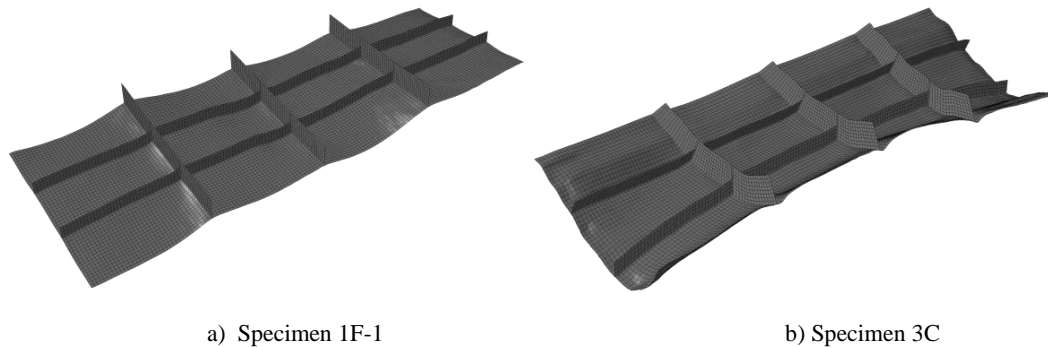


Fig. 25. Modelled initial geometry estimated with kriging (amplification factor 20).

In stiffened plated structures, residual stresses are mainly caused by welding, but in the case of curved plates, they also arise during the curving process. In the numerical model, only the longitudinal residual stresses caused by welding were considered by an idealized uniform stress distribution according to Smith [36], as shown in Fig. 26. The amplitude of tensile residual stresses near the weld is denoted with σ_y , while σ_c denotes the amplitude of compressive residual stresses. The total width of tensile residual stress zone is defined as $2\eta t$, where t is the thickness of the plate and η is a variable parameter depending on the geometry and welding conditions and usually ranges between 0.75 and 5 [36–40]. A recent investigation on HSS welded box section members performed by Somodi and Kövesdi [41] concluded that the amplitude of the tensile residual stress may be assumed equal to the yield strength for all steel grades up to S960. Hence, in the numerical model, equality $\sigma_y = f_y$ was assumed and compressive residual stresses σ_c were adequately calculated considering stress equilibrium in the cross-section. The residual stresses on the stiffeners were neglected. Parameter η was defined as $\eta = 1.25$, based on a simplification of the trapezoidal stress distribution proposed in the Swedish design code [39]. In a parametric study by Degée *et al.* [40], no obvious dependency of local slenderness on the influence of residual stresses on the overall member capacity was distinguished. Based on this observation, the parameter η was kept

constant for all plate configurations. The described residual stress distribution was implemented in the FE model by defining an initial stress condition and performing an equilibrating step before the static analysis.

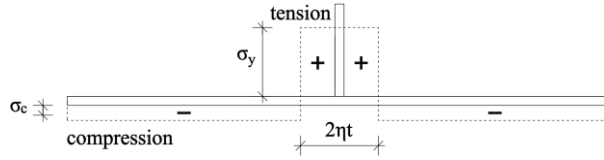


Fig. 26. Idealized longitudinal residual stress distribution in welded stiffened plate.

In Model 2, equivalent geometric imperfections were applied according to the recommendations from Annex C in EN 1993-1-5 [1]. The imperfection shapes were obtained from the buckling modes of the structure taken from a preliminary linear bifurcation analysis (LBA). For specimens with smaller aspect ratio α , the first buckling mode (local buckling of subpanels and stiffeners) was considered (two examples are given in Fig. 27). The magnitude of the imperfection was taken as $w_0 = \min(a/200, b_{loc}/200) = 0.95$ mm. For specimens 5C and 6C, a combination of global buckling mode as leading imperfection with magnitude $w_0 = \min(a/400, b/400) = 1.5$ mm and local buckling mode as accompanying imperfection reduced by 70% ($w_0 = 0.67$ mm) was considered. First elastic critical buckling loads $F_{cr,LBA}$ from LBA are listed in Table 3 for all specimens.

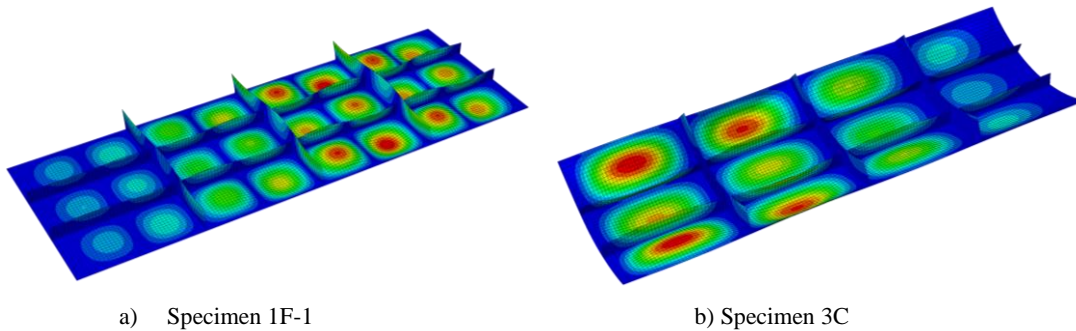


Fig. 27. First buckling mode shapes (amplification factor 20).

3.3 FEA results

3.3.1 Load versus axial shortening curves and ultimate resistance

Fig. 28 shows the load-shortening curves of the numerical simulations in comparison to the experimental ones. It has to be noted that vertical displacement v at the load application point plotted on the x axis is relatively small (around 4 mm at failure) and for this reason difficult to compare. In the numerical simulations, two models were considered, namely Model 1 and Model 2. In general, the achieved correlations of the global responses are reasonably good and the initial stiffnesses of the numerical models are more or less the same as those obtained from the tests. For curved specimens with the lowest relative slenderness, namely 1C-1, 1C-2 and 2C, both Model 1 and the experimental curve showed

ductile behaviour before failure. For all other specimens, however, the experimental ductile behaviour was not achieved with numerical simulations. Unlike experimental curves, the numerical response showed almost no post-critical strength reserve for specimens with slender subpanels, namely 3C-6C. A more detailed material model accounting for the curved part of the stress-strain curve (Fig. 24) would probably lead to better agreement between the results. The material model has more influence on the global response and ultimate resistance for plates with higher slenderness, where failure is mostly associated to buckling. The nonlinear elastic part of the standard tension test stress-strain curve is the consequence of a lower elastic modulus, leading to a plate more prone to buckling. This explains higher numerical capacity compared to test capacity for specimens 3C, 4C, 5C and 6C. Therefore, for HSS plated structures prone to stability phenomena, special attention has to be paid to the material model.

After reaching the ultimate strength, in most cases the discrepancy between the numerical and experimental curves was even larger. Numerical simulations were performed using arc-length method that allows to follow the load-shortening curve also in the post-buckling regime, where the load and displacement may both decrease along the loading path. On the other hand, the experimental tests were displacement controlled, resulting in an inevitable increase of the displacement.

In Table 3, the experimental test capacity (F_{test}) is compared against the ultimate resistances achieved by numerical simulations (F_{model1} , F_{model2}). In general, an overestimation of the ultimate resistance is achieved by numerical simulations, except for 1C-1 and 1C-2, where the maximum load obtained with Model 1 is in good correlation with the experimental value (difference is less than 2%). The average difference of 12 % between Model 1 and test results might be attributed also to additional imperfections that were not included in the modelling of realistic imperfections, such as stiffeners imperfections, uneven thickness of the plates, adjustments of the test layout during loading and imperfections at the level of boundary conditions that are difficult to measure. In most cases, the difference is smaller for Model 2, where the capacity is usually exhausted at smaller vertical deflection compared to the test results. Very good correlation is also achieved for flat specimens, namely 1F-1- and 1F-2, where the difference is 8 % for Model 1 and less than 3 % for Model 2. It may be concluded that the equivalent geometric imperfections give a good approximation of the realistic imperfections and can be considered in the finite element analysis of stiffened curved plates. However, it is sometimes difficult to find the most critical initial imperfection mode for stiffened plates without a detailed study of all possible modes.

Table 3. Load carrying capacity – comparison between experimental tests and numerical simulations.

Specimen	F_{test} [kN]	$F_{cr,LBA}$ [kN]	F_{model1} [kN]	F_{model1}/F_{test}	F_{model2} [kN]	F_{model2}/F_{test}
1C-1	2050	5085	2100	1.02	2031	0.99
1C-2	2145	5085	2129	0.99	2031	0.95
2C	1938	4990	2131	1.10	2043	1.05
3C	1138	2262	1419	1.25	1272	1.12
4C	1353	2385	1559	1.15	1417	1.05
5C	1113	2406	1336	1.20	1171	1.05

6C	1122	2519	1348	1.20	1244	1.11
1F-1	1805	2672	1923	1.07	1853	1.03
1F-2	1813	2672	1953	1.08	1853	1.02
			Average:	1.12	Average:	1.04
			St. dev.:	0.09	St. dev.:	0.05

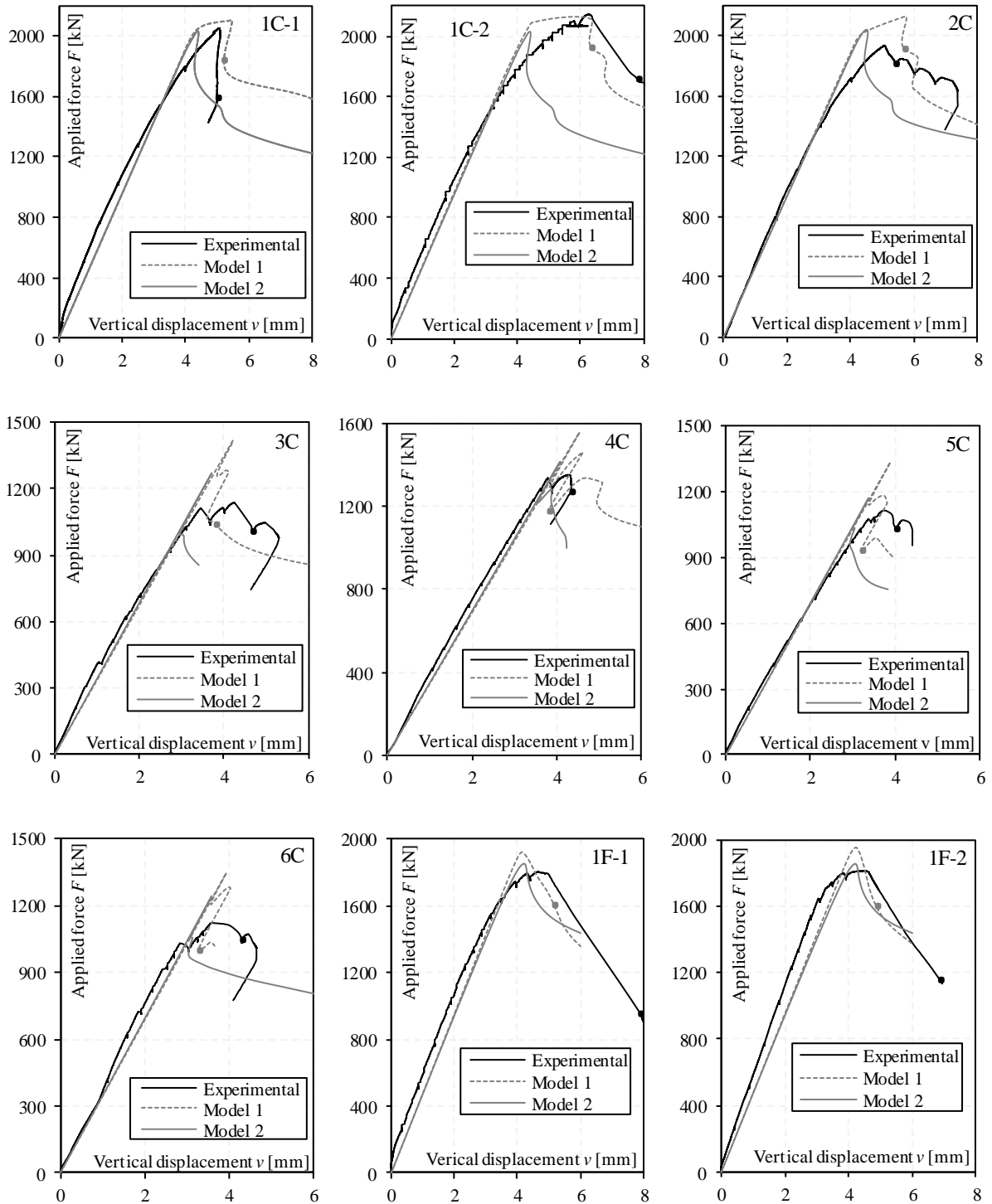
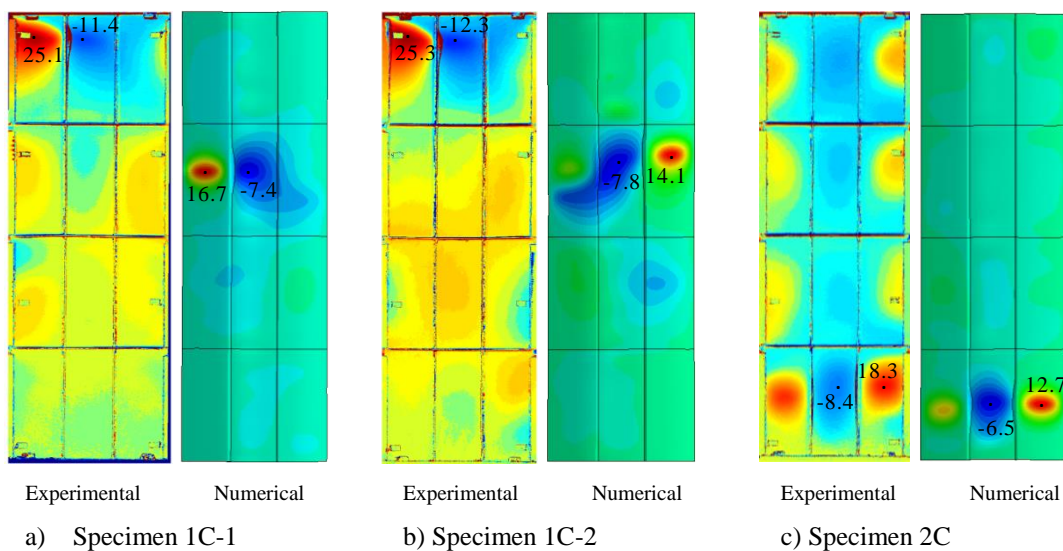


Fig. 28. Comparison of load-shortening curves.

3.3.2 Out-of-plane deflections and collapse mechanisms

In Fig. 29 the experimental and numerical collapse mechanisms are visualized by displaying the out-of-plane displacements at failure. The dots on the load-shortening curves in Fig. 28 denote the exact positions of the plotted displacements. With Model 1, which includes the realistic imperfections, a very good correlation with the experimental collapsed shapes is achieved, especially in the subpanels where higher deflections appear. Similar to experimental results, numerical analysis indicates that local collapse mechanism prevailed for all curved specimens in combination with torsional buckling of longitudinal stiffeners. For flat specimens 1F-1 and 1F-2, the bending failure mechanism may be observed as a consequence of the additional bending moment due to load eccentricity. Supported vertical edges of the numerical model attribute to the local bending mechanism, different from the global failure that arose in the experimental tests.

Despite the good agreement of deformed shapes, the differences in the maximum and minimum amplitudes are relatively high. In general, higher values were achieved with experimental tests. The differences may be attributed to different reasons. Due to the deviation in the experimental and numerical response curves after failure, the out-of-plane displacements are presented at different values of vertical displacement (see Fig. 28) and are for this reason not perfectly comparable. Namely, a large out-of-plane displacement may develop due to a small difference in vertical displacement v .



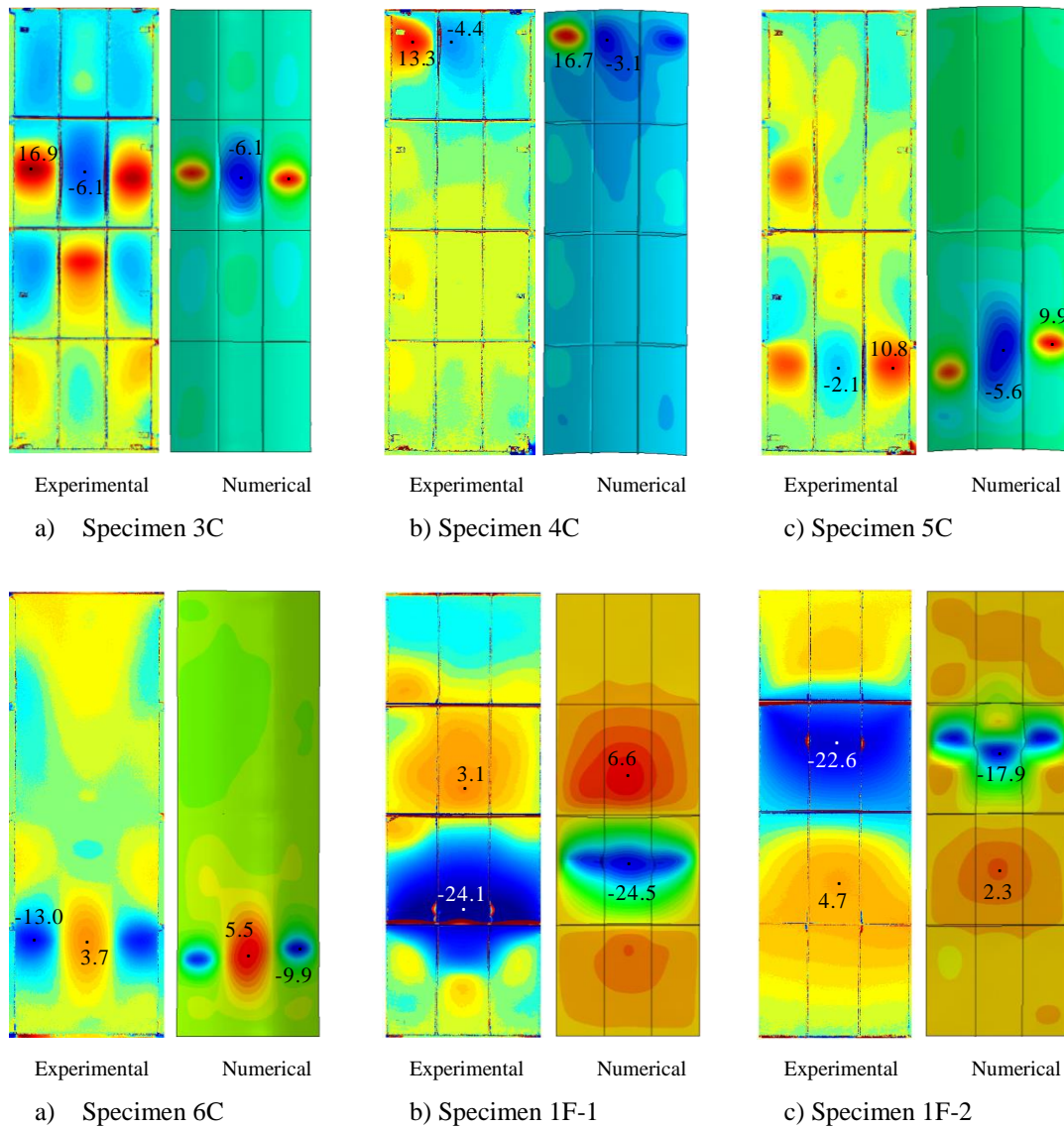


Fig. 29. Out-of-plane displacements at failure [mm] - experimental (left figures); numerical simulations with Model 1 (right figures).

3.3.3 Strains

Uniform compressive stresses in the specimen cross-section induced almost uniform strains along the panel cross-section in the elastic phase up to the manifestation of local buckling. This is presented for two representative specimens, namely 1C-1 and 3C in Figs. 30 and 31, respectively, where a comparison between numerical (Model 1) and experimental results is made. Strains are plotted at five different load levels. Continuous lines represent numerical results, dots represent six SG measurements. Up to a certain elastic strain level (approximately 2 ‰), the results show very good correlation. For higher plastic strains exhibited in specimen 1C-1, the deviation in the material model (Fig. 24) results in higher experimental values at load level $F = 1980$ kN. In experiment 1C-1, failure was concentrated in subpanel 1 (Fig. 29a), leading to different strains after failure in SGs Z7-Z9, compared to numerical results, where failure was concentrated in subpanel 4.

For specimen 3C, both the experimental and the numerical failures were concentrated in subpanels 4-6. In this case, the strains coincide perfectly and the numerical results confirm that for specimens with thinner panels, failure may be associated mostly with local buckling of subpanels. Specifically, the yield strain of 2.8 % was exceeded at some points of the panel only after the ultimate resistance had been reached.

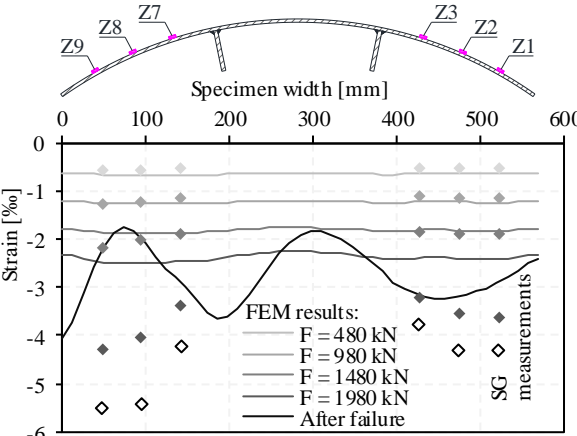


Fig. 30. Comparison of strain development, specimen 1C-1.

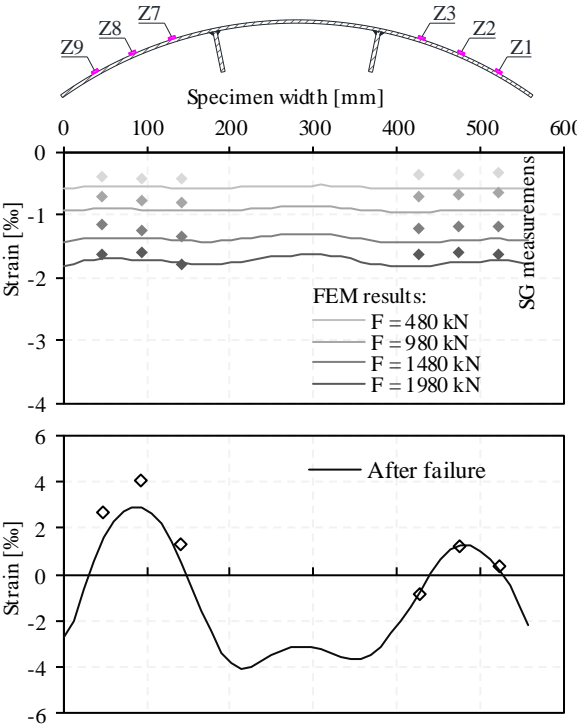


Fig. 31. Comparison of strain development, specimen 3C.

4 Verification of curved stiffened panels in pure compression

4.1 Verification according to EN 1993-1-5

The design of curved panels is not covered by the Structural Eurocodes. According to EN 1993-1-5, curved elements may be considered as flat, if the radius of curvature satisfies the limit given in Eq. (1). All curved panels included in this study exceed the limit considerably. Nevertheless, a comparison between experimental results and code provisions was performed in order to quantify the difference. The resistance was calculated according to the effective width method given in [1] for all specimens (Table 4). In the calculation, the curvature of the plate was neglected, the measured material values and plate thicknesses (Table 2) were considered and partial safety factors were omitted. According to [1], transverse stiffeners should provide a rigid support up to the ultimate limit state for a longitudinally stiffened plate by fulfilling the strength and the stiffness criteria. Numerical simulations showed that both criteria are met for all panels. Consequently, the buckling resistance to direct stresses might be restricted to longitudinally stiffened panels between transverse stiffeners, for which a two-step design procedure is proposed in [1]. Herein, the design rules for the resistance to direct stresses are briefly presented; more detail may be found in [42,43].

If the independent plated elements (subpanels, stiffeners) are class 4 sections, effective areas for local buckling of each plated element i need to be calculated:

$$A_{c,eff,loc,i} = \rho_{loc,i} A_{c,i} \quad (4)$$

where $\rho_{loc,i}$ is the reduction factor coming from a modified Winter formula [1]. $A_{c,i}$ are parts of A_c , which is the gross area of the compression zone except the edge panels of the stiffened plate A_{edge} . For the calculation of the plate slenderness, coefficient ε was taken as $\varepsilon = \sqrt{(235/R_{eH} [\text{MPa}])}$. In the second step, the reduction factors for plate-like ρ_p and column-like χ_c behaviour are calculated [1]. Finally, the reduction factor due to overall buckling of the whole stiffened panel ρ_c is interpolated between the respective reduction factors ρ_p and χ_c :

$$\rho_c = (\rho_p - \chi_c)\xi(2 - \xi) + \chi_c \quad (5)$$

For reduction factor χ_c , buckling curve c ($\alpha = 0.49$) is selected. ξ is calculated from the elastic critical plate-like stress $\sigma_{cr,p}$ and column-like buckling stress $\sigma_{cr,c}$:

$$\xi = (\sigma_{cr,p} / \sigma_{cr,c}) - 1 \quad (6)$$

In Table 4, the critical plate buckling stress $\sigma_{cr,p}$ corresponds to the occurrence of a one-wave global mode and was determined by using EBPlate freeware [44]. The critical column buckling stress $\sigma_{cr,c}$ was calculated by the classic Euler formula (see Equation 4.9, EN1993-1-5), considering the length of the column equal to the distance between transverse stiffeners.

The final effective area of a longitudinally stiffened plate subjected to uniform compression is:

$$A_{c,eff} = \rho_c A_{c,eff,loc} + A_{edge,eff} \quad (7)$$

The axial force acting on the cross-section retains its position during loading, whereas shift e_N of the centroid of the effective area occurs relative to the centre of gravity of the gross cross-section. This shift results in an additional bending moment $\Delta M = e_N F_u$ that was also considered in the calculation of the ultimate resistance $F_{u,EN}$.

Table 4. Estimated values of the design procedure according to EN 1993-1-5.

Specimen	A_c [cm ²]	$A_{c,eff,loc}$ [cm ²]	$\sigma_{cr,p}$ [kN/cm ²]	ρ_p	$\sigma_{cr,c}$ [kN/cm ²]	χ_c	ξ	ρ_c	$A_{c,eff}$ [cm ²]	$F_{u,EN}$ [kN]
1C	28.3	24.8	1561	1.0	1688	0.78	0.0	0.78	30.1	1629
2C	27.5	23.2	1398	1.0	1523	0.77	0.0	0.77	28.5	1591
3C	20.4	14.4	1647	1.0	1904	0.82	0.0	0.82	17.2	961
4C	20.4	12.6	1498	1.0	1719	0.78	0.0	0.78	15.0	1143
5C	21.4	15.8	456	0.80	501	0.55	0.0	0.55	14.0	795
6C	21.4	15.7	559	0.86	625	0.62	0.0	0.62	15.1	874
1F	28.3	24.8	1561	1.0	1688	0.78	0.0	0.78	30.1	1629

4.2 Proposed verification procedure for curved stiffened panels in pure compression

To follow the aforementioned design procedure by EN1993-1-5 and to account for the positive effects of panel curvature on the ultimate resistance, a combination of two different methodologies recently published by Martins *et al.* [15,16] and Tran *et al.* [7] is proposed.

Martins *et al.* [16] proposed a method (see Appendix) for computing the effective width of cylindrically curved panels based on a modified formula for the panel's critical stress [15] and reduction factor ρ_{loc}^* . The method is limited to short (aspect ratio $\alpha \leq 1.0$) curved panels with longitudinal edges unconstrained and loaded edges constrained with curvature parameter Z up to 100. The effective areas of each independent curved panel are calculated according to:

$$A_{c,eff,loc,i}^* = \rho_{loc,i}^* A_{c,i} \quad (8)$$

The effective areas of the flat elements, e.g. stiffeners, follow Eq. (4).

Tran *et al.* [7] proposed a methodology (see Appendix) neglecting the plate-like effects and considering only the column-like behaviour of the whole stiffened panel. The criterion provides an estimation of the ultimate strength on the safety side. The critical stress for column-like buckling $\sigma_{cr,c}^*$ should be obtained from the area and second moment of inertia of the whole curved stiffened cross-section, resulting in a modified reduction factor χ_c^* . The final effective area may be written as:

$$A_{c,eff}^* = \chi_c^* A_{c,eff,loc}^* + A_{edge,eff}^* \quad (9)$$

As the curvature has a very strong influence on the bending inertia of the stiffened panel, χ_c^* is higher compared to χ_c calculated according to [1], leading to a higher ultimate resistance F_u^* . According to Table 4, plate-like buckling does not have any effect on the ultimate resistance of the calculated cases. In Table 5, the values of the ultimate resistance according to the modified procedure are listed. It may be noticed that $A_{c,eff,loc}^*$ is in some cases smaller than $A_{c,eff,loc}$, as a consequence of lower local reduction coefficient ρ_{loc}^* of curved plates. Namely, local curvature parameter Z_{loc} of individual subpanels is in these cases relatively small. Thus, small curvature represents an additional imperfection of the plate that lowers the ultimate strength. This phenomenon is more pronounced for stockier panels and is covered in the modified formula for the panel's reduction factor ρ_{loc}^* proposed by Martins *et al.* [16].

Table 5. Estimated values of the proposed design procedure.

Specimen	$A_{c,eff,loc}^*$ [cm ²]	$\sigma_{cr,c}^*$ [kN/cm ²]	χ_c^*	F_u^* [kN]
1C	23.4	6745	0.97	1786
2C	21.8	6825	0.98	1759
3C	14.7	6444	0.98	1143
4C	12.9	6589	0.97	1373
5C	16.2	1534	0.85	1090
6C	16.1	1718	0.86	1117

4.3 Comparison of test results and verification procedures

In Table 6, the test capacity (F_{test}) and the numerical capacity (F_{model2}) are compared against the verification procedures described in Sections 4.1 and 4.2. For flat specimens, namely 1F-1 and 1F-2, the verification procedure according to EN 1993-1-5 gives a 10 % underestimation of ultimate resistance, even though measured material values and plate thicknesses were considered. The differences come from the effectiveness of the cross-section computed with the Winter formula. The formula accounts for favourable effects resulting from post-buckling plate behaviour and for detrimental effects of imperfections [42] and was calibrated versus test results by a statistical evaluation. Due to the difficulty in assessing the magnitude of edge restraints of subpanels between stiffeners, the conservative assumption of simply supported edges is made, resulting in the underestimation of the ultimate resistance. Moreover, factor ξ , that measures the vicinity of the elastic critical plate buckling stress to the elastic critical column buckling stress (Eq. (6)) and affects the interpolation of the reduction factor (Eq. (5)), is in all cases equal to 0 (see Table 4). Although it is physically impossible for $\sigma_{cr,p}$ to be smaller than $\sigma_{cr,c}$, the simplified concept of equivalent orthotropic plate used in EBPlate for $\sigma_{cr,p}$ computation, allows for the violation of this requirement. Therefore, the effectiveness of the stiffened panel is obtained only from the column buckling reduction factor neglecting any plate post-buckling resistance. At last, also the conservative assumption of the column-like buckling itself contributes to the ultimate resistance underestimation.

With an average difference of 21 %, EN 1993-1-5 gives smaller resistances compared to curved specimens' test results and 24 % lower results compared to numerical capacity. Therefore, current Eurocode rules are found safe in all the analysed cases and could cover the design of curved panels on the safety side by neglecting the curvature, as it was already numerically proven by Tran et al. [7].

The proposed verification procedure described in Section 4.2 gives a good estimation of the specimens' ultimate strength. In case of specimen 4C, a 1 % overestimation is calculated, while on average the difference is less than 6 %. Furthermore, compared to the numerical results, the proposed procedure is on the safe side for approximately 10 %. However, it has to be noted that a limited set of geometric parameters was included in the experimental study. Moreover, the method for computing the effective width of curved panels [16] is limited to aspect ratios $\alpha \leq 1$. Applying the method to subpanels of stiffened plates, like in the case of this study, the limit is easily exceeded. Hence, for the validation of the proposed procedure, an extensive parametric study has to be performed on a wide range of parameters.

Table 6. Comparison of load carrying capacity.

Specimen	F_{test} [kN]	F_{model2}	EN1993-1-5 (Section 4.1)			Proposed procedure (Section 4.2)		
			$F_{u,EN}$ [kN]	$F_{u,EN}/F_{test}$	$F_{u,EN}/F_{model2}$	F_u^* [kN]	F_u^*/F_{test}	F_u^*/F_{model2}
1F-1*	1805	1853	1629	0.90	0.88			
1F-2*	1813	1853	1629	0.90	0.88			
1C-1	2050	2031	1629	0.79	0.80	1786	0.87	0.88
1C-2	2145	2031	1629	0.76	0.80	1786	0.83	0.88
2C	1938	2043	1591	0.82	0.78	1759	0.91	0.86
3C	1138	1272	961	0.84	0.76	1143	1.00	0.90
4C	1353	1417	1143	0.84	0.81	1373	1.01	0.97
5C	1113	1171	795	0.71	0.68	1090	0.98	0.93
6C	1122	1244	874	0.78	0.70	1117	1.00	0.90
			Average:	0.79	0.76	Average:	0.94	0.90
			St. dev.:	0.05	0.05	St. dev.:	0.07	0.04

* Flat specimens are omitted from the average and standard deviation.

5 Conclusions and future work

Nine large scale panels stiffened with longitudinal and transverse stiffeners were tested under uniform compressive stresses. In practical bridge design this is a typical loading situation for bottom plates of box girders near internal supports. Both flat and curved panels were included in the study, all made of high strength steel. The aim of the tests was to examine the ultimate resistance and structural behaviour of transversally curved stiffened plates. In the range of the analysed parameters, the following remarks are made:

- The collapse mechanism of stiffened curved plates under compressive loads represents a complex engineering problem due to a combination of material, stiffener behaviour that comes from curvature, boundary conditions and plate slenderness.
- All specimens showed a linear elastic response up to a high load level. After local buckling failure, bending deformations were observed for flat panels due to the additional bending moment arising from load eccentricity. Higher section modulus prevented bending failure of curved specimens, for which local collapse mechanism prevailed in all cases in combination with torsional buckling of longitudinal stiffeners.
- For stockier panels, the ultimate load was mainly driven by the combination of local buckling and yielding of the material. For panels with higher slenderness, collapse behaviour was governed by elastic buckling and post-critical strength reserve.
- The ultimate force obtained by the flat panels was 13 to 19 % lower compared to the curved panels. Thus, introduction of curvature can add a resistance reserve to the stiffened panels. Furthermore, the ultimate resistance remained nearly constant regardless of the increased aspect ratio.

Two numerical models were built and verified against the test results. In general, reasonably good correlation is achieved between numerical and experimental results regarding initial stiffness and failure shape. The ultimate strength is in better agreement with the numerical model where equivalent geometric imperfections were assumed (Model 2). Thus, equivalent geometric imperfections give a good approximation of the realistic imperfections and they will be further considered in the finite element analysis of stiffened curved plates. For further work, a more accurate material model has to be used to account for nonlinear effects typical for HSS, especially when plated structures prone to stability phenomena are under consideration.

The verification according to the effective width method given in EN 1993-1-5 proves to be conservative for all tested configurations. Therefore, with a significant underestimation, current Eurocode rules could cover the design of curved panels by neglecting the curvature. For the two flat specimens, a 10 % underestimation by the method was found, arising from some conservative assumptions and simplified concepts included in the verification procedure. An alternative verification procedure for curved stiffened panels is proposed that is in line with the original concept of EN1993-1-5, accounting for panel

curvature. The procedure gives a good estimation of the specimens' ultimate strength with an average difference less than 6 %.

The conclusions are made based on the test data obtained from the experiments and are therefore limited to specimens similar to those used in this study. To verify the procedure for an arbitrary stiffened curved panel, an extensive parametric study will be carried out. Future trends of bridge structures are oriented to even fewer longitudinal stiffeners with higher flexural and torsional rigidity. Therefore, trapezoidal stiffeners will be included in the parametric study together with a wide range of other significant geometric parameters.

Acknowledgments

The research was carried out under the financial support from the European Commission's Research Found for Coal and Steel through the research project OUTBURST (RFCS-2015-709782) and national funds from Slovenian Research Agency ARRS within the project P2-0158. Their support is gratefully acknowledged.

Appendix

According to Martins *et al.* [15], the elastic critical stress of cylindrically curved panels subjected to uniform compression is obtained with:

$$\sigma_{cr} = C_l k_\sigma \frac{\pi^2 E}{12(1-\nu^2)} \left(\frac{t}{b}\right)^2 \quad (\text{A.1})$$

where k_σ is the elastic buckling coefficient defined in Table A.1 and C_l is a correction factor for long panels defined in Table A.2.

Table A.1. Elastic buckling coefficient for short curved panels under uniform compression

	$k_\sigma = \frac{a_1 + a_2 Z + a_3 Z^2}{b_1 + b_2 Z + b_3 Z^2}$	
	$a_1 = 8.2$	$b_1 = 1.05$
$0 < Z \leq 23$	$a_2 = 0.0704$	$b_2 = -0.0002$
	$a_3 = 0.0163$	$b_3 = 0.0003$
	$a_1 = 3.214$	$b_1 = 0.961$
$23 < Z \leq 100$	$a_2 = 0.5976$	$b_2 = 0.0104$
	$a_3 = 0.0028$	$b_3 = 0$

Table A.2. Correction factor C_i

	$\alpha > 1$	$\alpha \leq 1$
$Z = 5$	1.00	
$Z = 40$	1.08	1.00
$Z = 100$	1.13	

In Martins *et al.* [16], the effective width reduction factor is evaluated from the following formulae:

$$\begin{aligned}
\rho_{loc,i}^* &= 1 & \text{if } \bar{\lambda} &\leq \bar{\lambda}_{0,Z} \\
\rho_{loc,i}^* &= \frac{\bar{\lambda}_{0,p} - \bar{\lambda} + \rho_{0,Z}(\bar{\lambda} - \bar{\lambda}_{0,Z})}{\bar{\lambda}_{0,p} - \bar{\lambda}_{0,Z}} & \text{if } \bar{\lambda}_{0,Z} < \bar{\lambda} < \bar{\lambda}_{0,p} \\
\rho_{loc,i}^* &= \frac{\bar{\lambda} - 0.22a_Z}{c_Z \bar{\lambda}^2} + S_Z & \text{if } \bar{\lambda} \geq \bar{\lambda}_{0,p}
\end{aligned} \tag{A.2}$$

where:

$$\bar{\lambda} = \sqrt{\frac{f_y}{\sigma_{cr}}} \tag{A.3}$$

$$\rho_{0,Z} = \frac{\bar{\lambda}_{0,p} - 0.22a_Z}{c_Z \bar{\lambda}_{0,p}^2} + S_Z \tag{A.4}$$

and $\bar{\lambda}_{0,p} = 0.673$. All other parameters are listed in Table A.3 and are obtained by a linear interpolation.

According to Tran *et al.* [45], $\bar{\lambda}_{0,Z}$ is defined as:

$$\bar{\lambda}_{0,Z} = 0.2 + 0.473(0.95^Z) \tag{A.5}$$

Table A.3. Values of numerical parameters a_z , c_z and S_z .

	$Z = 0$	$Z = 10$	$Z = 23$	$Z = 100$
a_z	1.000	1.000	1.000	0.545
c_z	1.000	1.290	1.150	1.700
S_z	0.000	0.060	-0.040	-0.040

Following the methodology proposed by Tran *et al.* [7] and accounting for the effective area of the curved panel $A_{c,eff,loc}^*$ calculated in the previous step, the modified column buckling reduction factor χ_c^* is obtained from:

$$\chi_c^* = \frac{1}{\phi + \sqrt{\phi^2 - \bar{\lambda}_c^2}} \quad \text{with} \quad \phi = 0.5 \left[1 + \alpha_e (\bar{\lambda}_c - 0.2) + \bar{\lambda}_c^2 \right] \tag{A.6}$$

where α_e is evaluated from the standard Eurocode procedure and the buckling curve is selected according to the shape of longitudinal stiffeners. The reduced column slenderness $\bar{\lambda}_c$ is calculated from the elastic critical column buckling stress $\sigma_{cr,c}^*$.

$$\bar{\lambda}_c = \sqrt{\frac{A_{c,eff,loc}^*}{A^*} \frac{f_y}{\sigma_{cr,c}^*}} \quad (\text{A.7})$$

$$\sigma_{cr,c}^* = \frac{\pi^2 EI_y^*}{A^* a^2} \quad (\text{A.8})$$

The length of the column a equals the distance between transverse stiffeners. The area A^* and second moment of inertia I_y^* must be evaluated on the whole cross-section as shown in Fig. A.1.

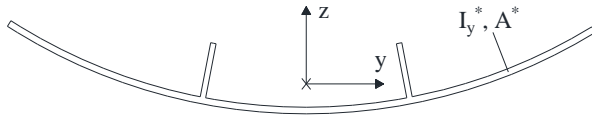


Fig. A.1. Geometric parameters of the whole stiffened curved cross-section.

6 References

- [1] CEN, EN 1993-1-5:2006 - Eurocode 3: Design of steel structures, Part 1-5: Plated Structural Elements, Brussels: European Committee for Standardization, 2006.
- [2] A. Biscaya da Graça, J. Oliveira Pedro, J.P. Martins, A. Reis, Estado da arte em pontes incluindo painéis metálicos cilíndricos na secção transversal, in: XI Congr. Construção Metálica e Mista, Coimbra, Portugal, 2017.
- [3] M.J. Pantaleón, Ó.R. Ramos, G. Ortega, J.M. Martínez, F. Schanack, Dynamic Analysis of a Composite Cable-Stayed Bridge: Escaleritas Viaduct, *J. Bridg. Eng.* 15 (2010) 653–660. doi:10.1061/(ASCE)BE.1943-5592.0000116.
- [4] A. Reis, J. Oliveira Pedro, A. Biscaya da Graça, Report on the comparative study 1: alternative cross-section integrating curved stiffened steel panels. RFCS Research Project OUTBURST (RFCS-2015-709782): Deliverable 3.3, 2017.
- [5] J.P. Martins, D. Beg, F. Sinur, L. Simões Da Silva, A. Reis, Imperfection sensitivity of cylindrically curved steel panels, *Thin-Walled Struct.* 89 (2015) 101–115. doi:10.1016/j.tws.2014.12.014.
- [6] S. Piculin, F. Sinur, P. Može, Analysis of stiffened curved panels in compression: A preliminary numerical study for experimental tests, in: Proc. Eurosteel 2017, Copenhagen, Denmark, 2017.
- [7] K.L. Tran, C. Douthe, K. Sab, J. Dallot, L. Davaine, Buckling of stiffened curved panels under uniform axial compression, *J. Constr. Steel Res.* 103 (2014) 140–147. doi:10.1016/j.jcsr.2014.07.004.
- [8] F. Ljubinković, J.P. Martins, H. Gervásio, L. Simões da Silva, Ultimate load of cylindrically curved steel panels under pure shear, *Thin-Walled Struct.* 142 (2019) 171–188. doi:10.1016/j.tws.2019.04.022.
- [9] J. Oliveira Pedro, A. Reis, C. Baptista, High Strength Steel S690 in highway bridges, *Stahlbau.* 87 (2018) 555–564. doi:10.1002/stab.201810615.
- [10] B. Kövesdi, L. Dunai, C. Hendy, Minimum requirements for transverse stiffeners on orthotropic plates subjected to compression, *Eng. Struct.* 176 (2018) 396–410. doi:10.1016/j.engstruct.2018.09.019.
- [11] R. Maquoi, M. Skaloud, Stability of plates and plated structures: General Report, *J. Constr. Steel Res.* 55 (2000) 45–68. www.elsevier.com/locate/jcsr.
- [12] J.P. Martins, F. Ljubinkovic, L. Simões da Silva, H. Gervásio, Behaviour of thin-walled curved steel plates under generalised in-plane stresses: A review, *J. Constr. Steel Res.* 140 (2018) 191–207. doi:10.1016/j.jcsr.2017.10.018.
- [13] J.K. Seo, C.H. Song, J.S. Park, J.K. Paik, Nonlinear structural behaviour and design formulae for calculating the ultimate strength of stiffened curved plates under axial compression, *Thin-Walled Struct.* 107 (2016) 1–17. doi:10.1016/j.tws.2016.05.003.
- [14] J.-S. Park, K. Iijima, T. Yao, Buckling/ultimate strength and progressive collapse behaviour comparison

- of unstiffened and stiffened curved plates subjected to axial compression, *Int. J. Comput. Appl. Technol.* 41 (2011) 60–72. doi:<https://doi.org/10.1504/IJCAT.2011.042233>.
- [15] J.P. Martins, L. Simões Da Silva, A. Reis, Eigenvalue analysis of cylindrically curved panels under compressive stresses - Extension of rules from en 1993-1-5, *Thin-Walled Struct.* 68 (2013) 183–194. doi:10.1016/j.tws.2013.03.010.
- [16] J.P. Martins, L. Simões Da Silva, A. Reis, Ultimate load of cylindrically curved panels under in-plane compression and bending - Extension of rules from en 1993-1-5, *Thin-Walled Struct.* 77 (2014) 36–47. doi:10.1016/j.tws.2013.11.012.
- [17] K.L. Tran, C. Douthe, K. Sab, J. Dallot, L. Davaine, A preliminary design formula for the strength of stiffened curved panels by design of experiment method, *Thin-Walled Struct.* 79 (2014) 129–137. doi:10.1016/j.tws.2014.02.012.
- [18] K. Ghavami, M.R. Khedmati, Numerical and experimental investigations on the compression behaviour of stiffened plates, *J. Constr. Steel Res.* 62 (2006) 1087–1100. doi:10.1016/j.jcsr.2006.06.026.
- [19] J.M. Gordo, C.G. Soares, Compressive tests on stiffened panels of intermediate slenderness, *Thin-Walled Struct.* 49 (2011) 782–794. doi:10.1016/j.tws.2011.02.004.
- [20] F. Sinur, A. Zizza, U. Kuhlmann, D. Beg, Buckling interaction of slender plates - Experimental and numerical investigations, *Thin-Walled Struct.* 61 (2012) 121–131. doi:10.1016/j.tws.2012.03.024.
- [21] F. Sinur, D. Beg, Moment-shear interaction of stiffened plate girders - Tests and numerical model verification, *J. Constr. Steel Res.* 85 (2013) 116–129. doi:10.1016/j.jcsr.2013.03.007.
- [22] S.R. Cho, H.Z. Park, H.S. Kim, J.S. Seo, Experimental and numerical investigations on the ultimate strength of curved stiffened plates, in: *Proceeding 10th Int. Symp. Pract. Des. Ships Other Float. Struct.*, 2007. <https://www.researchgate.net/publication/289700911>.
- [23] F. Ljubinkovic, J.P. Martins, H. Gervásio, L. Simões Da Silva, C. Leitao, Experimental analysis of unstiffened cylindrically curved panels, in: *XI Conf. Steel Compos. Constr.*, Coimbra, Portugal, 2017. doi:10.1002/cepa.544.
- [24] F. Ljubinković, J.P. Martins, H. Gervásio, L.S. da Silva, J.O. Pedro, Experimental behavior of curved bottom flanges in steel box-girder bridge decks, *J. Constr. Steel Res.* 160 (2019) 169–188. doi:10.1016/j.jcsr.2019.05.031.
- [25] S.B. Batdorf, A simplified method of elastic-stability analysis for thin cylindrical shells, National Advisory Committee for Aeronautics, Technical Note number: 1342, 1947.
- [26] CEN, Metallic materials - Tensile testing - Part 1: Method of test at room temperature. ISO 6892-1:2016, 2016.
- [27] A. Zizza, Buckling behaviour of unstiffened and stiffened steel plates under multiaxial stress states, Ph.D. thesis, University of Stuttgart, 2016.
- [28] V. Pourostad, A. Zizza, U. Kuhlmann, Investigations on the Buckling Behaviour of Slender High Strength Steel Plates under Multiaxial Stresses, in: *Proc. Eurosteel 2017*, Copenhagen, Denmark, 2017. doi:10.1002/cepa.128.
- [29] D. Grigillo, J. Snoj, M. Dolšek, Photogrammetric measurement of deformations in tests of mechanical resistance of structural elements, *Geod. Vestn.* 60 (2016) 13–27.
- [30] M. Mahendran, Local plastic mechanisms in thin steel plates under in-plane compression, *Thin-Walled Struct.* 27 (1997) 245–261. doi:10.1016/S0263-8231(96)00040-7.
- [31] R. Timmers, G. Lener, Collapse mechanisms and load–deflection curves of unstiffened and stiffened plated structures from bridge design, *Thin-Walled Struct.* 106 (2016) 448–458. doi:10.1016/j.tws.2016.05.020.
- [32] ABAQUS FEA, DS Simulia, Dassault Systems, Version 6.14, (2017).
- [33] L. Gardner, D.A. Nethercot, Numerical Modeling of Stainless Steel Structural Components—A Consistent Approach, *J. Struct. Eng.* 130 (2004) 1586–1601. doi:10.1061/(ASCE)0733-9445(2004)130:10(1586).
- [34] D.G. Krige, A statistical approach to some basic mine problems on the Witwatersrand, *J. Chem. Metall. Min. Soc. South Africa.* 52 (1951) 119–139.
- [35] M.A. Oliver, R. Webster, A tutorial guide to geostatistics: Computing and modelling variograms and kriging, *Catena.* 113 (2014) 56–69. doi:10.1016/j.catena.2013.09.006.
- [36] M.J. Smith, Ultimate strength assessment of naval and commercial ships, Defence Research and Development Canada, 2008.
- [37] L. Gannon, Y. Liu, N. Pegg, M.J. Smith, Effect of welding-induced residual stress and distortion on ship

- hull girder ultimate strength, *Mar. Struct.* 28 (2012) 25–49.
- [38] B.Q. Chen, C. Guedes Soares, Effects of plate configurations on the weld induced deformations and strength of fillet-welded plates, *Mar. Struct.* 50 (2016) 243–259. doi:10.1016/j.marstruc.2016.09.004.
- [39] Swedish Regulations for Steel Structures, BSK 99, National Board of Housing, Building and Planning, 2003.
- [40] H. Degée, A. Detzel, U. Kuhlmann, Interaction of global and local buckling in welded RHS compression members, *J. Constr. Steel Res.* 64 (2008) 755–765. doi:10.1016/j.jcsr.2008.01.032.
- [41] B. Somodi, B. Kövesdi, Residual stress measurements on welded square box sections using steel grades of S235–S960, *Thin-Walled Struct.* 123 (2018) 142–154. doi:10.1016/j.tws.2017.11.028.
- [42] B. Johansson, R. Maquoi, G. Sedlacek, New design rules for plated structures in Eurocode 3, *J. Constr. Steel Res.* 57 (2001) 279–311. doi:10.1016/S0143-974X(00)00020-1.
- [43] U. Kuhlmann, A. Zizza, B. Braun, H. Degée, New chances and developments of Eurocode 3 Part 1.5 - Bridge design aspects, *Steel Constr.* 4 (2011) 224–231. doi:10.1002/stco.201110030.
- [44] CTICM, EBPlate, Piece of Software for the determination of elastic critical stresses in plates. EBPlate can be downloaded for free from www.cticm.com, (2007).
- [45] K. Le Tran, L. Davaine, C. Douthe, K. Sab, Stability of curved panels under uniform axial compression, *J. Constr. Steel Res.* 69 (2012) 30–38. doi:10.1016/j.jcsr.2011.07.015.